THE EFFECT OF CHANGES IN FREEZING RATES ON PRIMARY DENDRITE SPACING IN DIRECTIONALLY SOLIDIFIED DILUTE ALLOYS OF BISMUTH IN TIN

by

P. RAVI KUMAR

DEPARTMENT OF METALLURGICAL ENGINEERING

INDIAN INSTITUTE OF TECHNOLOGY, KANPUR

AUGUST, 1991

THE EFFECT OF CHANGES IN FREEZING RATES ON PRIMARY DENDRITE SPACING IN DIRECTIONALLY SOLIDIFIED DILUTE ALLOYS OF BISMUTH IN TIN

A Thesis Submitted
In Partial Fulfilment of the Requirements
for the Degree of

MASTER OF TECHNOLOGY

by
P. RAVI KUMAR

to the

DEPARTMENT OF METALLURGICAL ENGINEERING
INDIAN INSTITUTE OF TECHNOLOGY, KANPUR
AUGUST, 1991

C E R T I F I C A T E

It is certified that the work contained in the thesis entitled "**Effect of Changes in freezing rates on primary dendrite spacing in directionally solidified dilute alloys of bismuth in tin**" by "**P. Ravikumar**" has been carried out under my supervision and that it has not been submitted elsewhere for a degree.

(V. Bansal)
Associate Professor
Department of Metallurgical Engineering
Indian Institute of Technology
Kanpur - 208016

Date : August, 1991

ACKNOWLEDGEMENTS

I take this opportunity to express my deepest sense of gratitude to Dr. V. Bansal, Professor, Department of Metallurgical Engineering, I.I.T., Kanpur for suggesting this topic and for his constant guidance and encouragement throughout the course of this work. I also express my hearty gratitude to Mr. G.S. Sharma, Lab Technician, Mr. V.P. Gupta, Draftsman, Mr. Pant, Typist and friends Sri S.K. Singh, Sri V.C.V Rao, Sri M. Jawed, Sri A.K. Arora, Sri D. Prakash, Sri S.C.S. Rao and others who helped in preparing this thesis.

P. Ravikumar

August, 1991

Table of contents

List of Figures

List of Tables

ABSTRACT

The present work involves microstructual study and dendrite arm spacing measurement of directionally solidified Sn-Bi alloys. The alloy compositions have been chosen as 1,2 and 4 wt% Bi in order to primarily have single phase dendritic growth.

Directional solidification was carried out by moving the furnace relative to the quartz crucible (held stationary) containing the alloy at rates between 25 to 300 μm/S. Sudden changes (either infinite acceleration or deceleration) in rate of freezing have been introduced after every 0.02 to 0.03 meters of solidification at one particular rate of freezing.

It's observed that the adjustment of spacing in response to the freezing rate change was more immediate initially and then it gradually reached a new steady state value. It's also observed that the total time taken for readjustment incase of infinite deceleration was more compared to the infinite acceleration in freezing rate.

CHAPTER 1

INTRODUCTION

Directional solidification has been enjoying the attention and interest of numerous investigators since nearly four decades. On the science side it has enhanced our understanding of solidification process by constantly assisting us in quantifying and predicting related phenomenon, on the engineering side it has wide applications in controlling solidification so as to produce materials of immense variety more economically, with improved properties and performance characteristics.

The spectrum of investigations has ranged from the macroscopic to the submicroscopic. On the macroscopic scale the problems are concerned with ingot or casting design or problems of macrosegregation. On the microscopic scale people are concerned with grain size, their shape, distribution and orientation. On a finer scale, attention has been paid to dendritic structure and microsegregation within the grains. On a still finer scale, attempts have been made to reach finally the atomic level, where one is concerned with the nature of solid-liquid interface and the kinetics of attachment of new atoms during solidification.

At all these levels, excellent science has been underway and the technological achievements have been significant. Through directional solidification the movement of a stable and plane solid-liquid interface produced single crystals for computer chips and solar cells. Perfectly

aligned laminated composite structures have been possible through directional solidification in order to impart superior properties in superalloys[1] such as high strength, durability and reliable performance in high temperature applications. Production of high strength permanent magnets and superconducting[2] materials are other fields of applications.

Computers have played a significant role in the rapid evolution of directional solidification processing methods[3]. Investigation in directional solidification has also extended our control over volume fractions of constituent phases during solidification and thus producing lamellar eutectic structure from off-eutectic composition.

In many of these applications it is the fineness in dendritic structure that has produced stronger and more ductile castings. In fact the dendritic arm spacing is the most important factor in describing dendritic structures, which has correlated best with the engineering properties and homogenization kinetics. People have reported many a factors which affect the dendrite spacing such as temperature gradient, solidification rate local cooling rate, solute type and its concentration etc. Attempts for theoretical prediction of arrayed structures in which dendrites usually appear have not been very successful. Many adhoc principles such as minimum undercooling or maximum velocity or minimum entropy production have been adopted in order to explain the experimental data without much reasoning. Stability criterion is the latest development in this direction.

1.1 Lamellar growth theoretical :

It is assumed that the rate of advance of the interface[4] is imposed by the conditions of growth, and that the widths of the lamellae adjust themselves to steady state values. Tiller[5] following a treatment by Zener[6] shows that the lamellar width is determined by the interaction of two opposing free energy considerations : One is that the transverse diffusion of the solutes must occur over greater distances for thicker lamellae, and therefore a larger driving force is required, and the other is that the presence of interphase boundaries increases as the lamellar width decreases : thus the diffusion condition tend towards thin lamellae, while the surface energy of the interfaces favours thick lamellae. The amount of transverse diffusion that is required per unit time increases as the speed of growth increases for a given lamellar thickness, therefore higher speed with less time for diffusion produces thinner lamellae.

Directional solidification is important in eutectic solidification. The directional freezing technique has been applied extensively to turbine blade manufacture. Directional solidification promotes a texture i.e. dendrites grow in a preferred direction. The columnar structures avoid transverse grain boundaries which are an initiating point for creep failure.

1.2 Lamellar spacing adjustment with changes in growth velocity :

Experimentally the lamellar spacing of a eutectic depends on growth rate. Theoretically however for a given

spacing, a range of growth rates are possible. It has been proposed that eutectics grow within the stable range with the spacing controlled by the movement of lamellar faults.

The formation and general characteristics of lamellar faults have been described by Dean, H. et. al[7]. The main concern is at their movement and their role in interlamellar spacing changes. Serial sectioning methods were used to study the spacing changes. The studies confirmed that extensive lamellar terminations and fault line movement occurs during steady state growth without changing the average interlamellar spacing. Double's[8] microstructural studies show that lamellar terminations are not effective in changing the spacing. Terminations are relatively immobile compared to the marked flexibility of movement of fault lines.

When complex shapes like gas turbine blades[9] are directionally solidified, it is inevitable that cross-sectional area changes will lead to sudden fluctuations in the growth velocity. Farag and Neff[10] have examined the influence of sudden changes in growth velocity on the structure of Ni-Al-Nb composites. They have shown that such changes lead to the breakdown of planar to cellular eutectic coupled growth, banding or a change in the grain size of the component. These growth irregularities are detrimental to composite properties. So it is important to study the dendrite spacing changing mechanism with sudden changes in growth velocities.

The present work is an attempt towards the above objective. It has been aimed at microstructural study and

dendrite arm spacing measurement of directionally solidified Sn-Bi alloys. The alloy compositions have been chosen as 1,2 and 4 wt pct Bi so as to be considerably lower than the maximum solid solubility in order to primarily have single phase dendritic growth. Unidirectional solidification has been achieved by maintaining a fairly constant pre-set temperature gradient i.e. around 13^{o}c/mm.

Directional solidification is carried out by moving the furnace relative to the quartz crucible (held stationary) containing the alloy at rates between 25 to 300 μm/s. Sudden changes (infinite acceleration) in rate of freezing have been introduced after every 0.02 to 0.03 meters of solidification at one particular rate of freezing.

CHAPTER 2

EQUIPMENT AND EXPERIMENTAL SET UP

The present work was carried out in an existing experimental set-up[11,12]. It consists of a number of units and accessories to carry out master alloy preparation and directional solidification.

2.1 Directional solidification unit :

Solidification becomes unidirectional when heat is extracted from a solidifying specimen along one direction only. Fig. 2.1 is a schematic diagram of the directional solidification apparatus. In this apparatus, the furnace and the chill ring are moved with respect to a stationary specimen. The moving chill ring ensures constant thermal gradients in front of the solid/liquid interface throughout the run. This arrangement also prevents the solidifying specimen from any sort of mechanical disturbance that would otherwise occur if the specimen itself were to move. The ingot is made to directionally solidify starting from its bottom towards the top.

2.1.1 The driving mechanism :

In the solidification unit the driving mechanism (as shown in Fig. 2.1) is the sole cause of the solidification to proceed unidirectionally. The temperature gradient (maintained by the furnace - chill assembly) was effectively moved past the static specimen by means of this.

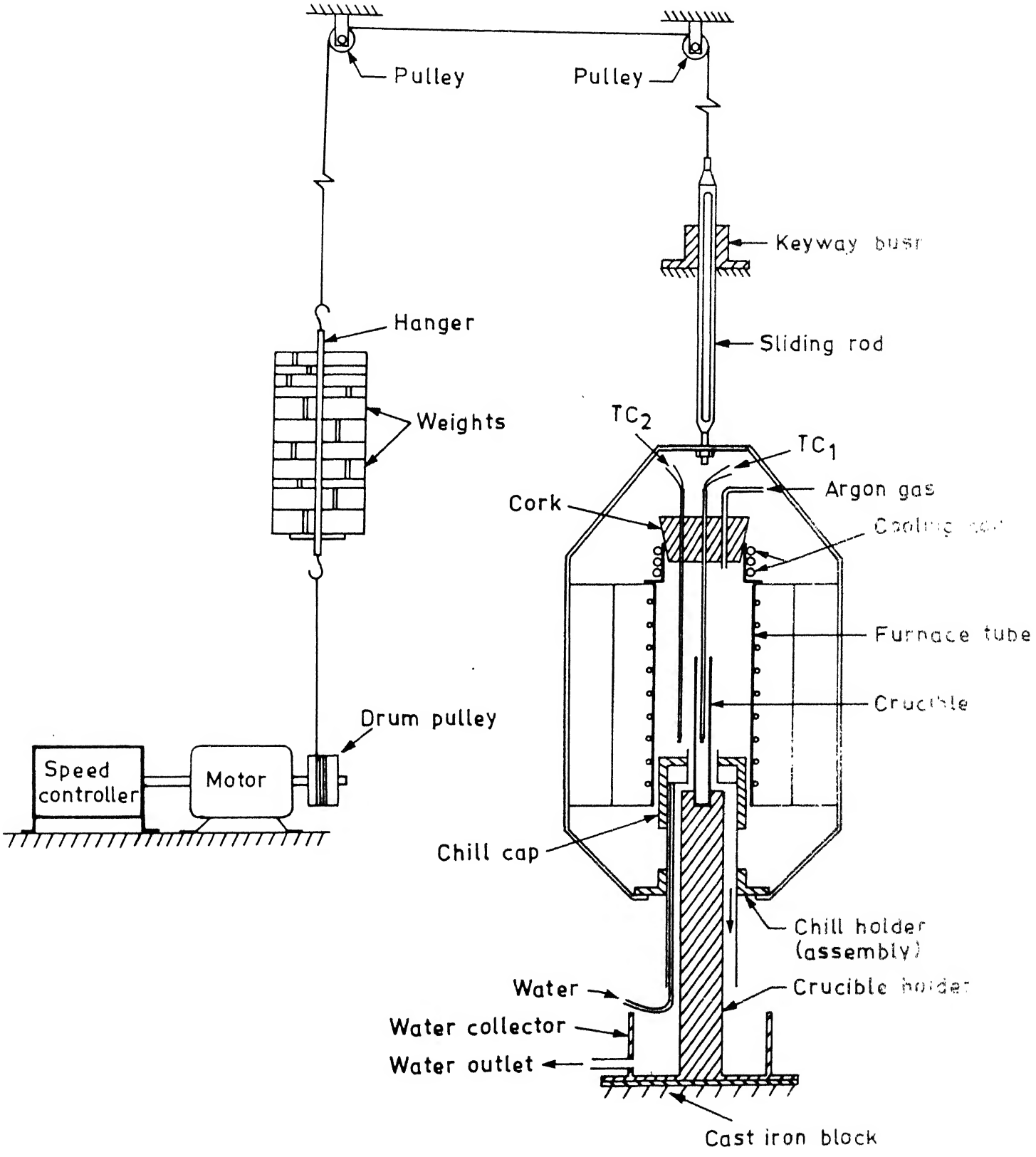

Fig. 2.1. Schematic diagram of the apparatus used in the present work.

There was a slotted steel rod hanging from a flexible wire rope to which the furnace was rigidly bolted. The other end of the wire-rope was attached to the drum pulley of a motor via a counter weight to counter balance the weight of the furnace. The movement of the steel rod was restricted to a vertical line by pulling it through a brass guide block fixed rigidly to the frame of the unit. A rectangular key inside the guide block prevented the furnace from axial rotation by fitting itself well into the slot of the steel rod. The motor assembly was capable of providing a wide range of speeds. The speed of the motor was controlled by a controller in which there is a ten turn potentiometer head. By rotating the head the speed of the motor was changed. The direction of rotation of the motor is reversible so that the furnace can be moved up and down

2.1.2 The crucible stand :

A cylindrical quartz crucible containing the specimen was held along the furnace axis by means of a stand (shown in Fig. 2.1). It was a brass rod mounted on a metallic base plate and there was a blind hole on its top end into which the quartz crucible has to sit. The crucible was held firmly by means of three screws fitted into the wall of the blind hole. This stand is slender enough to project the crucible well into the furnace. A metallic cup with a drain pipe was there on the base plate and encircling the crucible stand to collect the water coming out of the chill device. The stand was placed on a cast iron block. The base plate was screwed rigidly to the cast iron block. This prevented

any stray vibrations from the ground effecting the crucible stand.

2.2 Master alloy making facility :

2.2.1 Rocking furnace :

It is a sixty centimeter long cylindrical resistance wound furnace[13] with internal diameter of three centimeters. The furnace is held by diametrically opposite two horizontal pivots. It can be rocked from a vertical position down below the horizontal line through an angle of 120^{o} and can be clamped at any convenient position within an angle of approximately 20^{o} on either side of the horizontal position. It is capable of providing an effective heating zone of fifty centimeters length. The maximum safe operating temperature attainable in this furnace is around 850^{o}c. One end of the furnace was closed temporarily by clamping a small piece of metallic plate. A clamping mechanism to hold the capsule securely was provided at the other end. A thermocouple with its tip close to the resistance winding at the middle of the furnace was provided to measure the operating temperature.

2.2.2 Master alloy making :

Tin and bismuth have a specific densities of 7.3. and 9.8 respectively. Special measures were taken for preparing the master alloy. Melting and thorough mixing were possible in the above mentioned rocking furnace by putting the charge into it in a capsule. The capsule was sealed at one end and through the other end it was connected to

purified argon supply and vacuum pump by means of a two way stop cock. Initially the bulb was completely evacuated and then argon was allowed in. This process of evacuation and back filling with argon was carried out three to four times before the charge melts. This way any traces of air were removed from the capsule. The furnace was rocked several times after the charge had melted thoroughly at a super heat of around 70^{o}c. This ensured thorough mixing in the melt. Finally the capsule was held in a vertical position keeping the crucible mold portion of the crucible at the bottom. This crucible mold portion containing the melt was quenched in water. This resulted in producing a cylindrical alloy ingot of exact composition without much segregation or any impurity contamination. Later the bulb portion of the capsule was chopped off from the crucible carrying the ingot for subsequent use.

2.2.3 Specimen capsules :

The specimen capsules (as shown in Fig. 2.2) were prepared in which the melting, ingot casting and finally the directional solidification was carried out. A capsule consisted of two parts - a bulb portion and a cylindrical mold made out of quartz tubes. The cylindrical end was sealed. 99.995% purity tin and 99.9998% purity bismuth nodules in exact proportion were weighed in an electronic digital balance and were filled into the capsule. After melting, mixing and ingot casting the bulb portion of the capsule was cut off and saved to be reused.

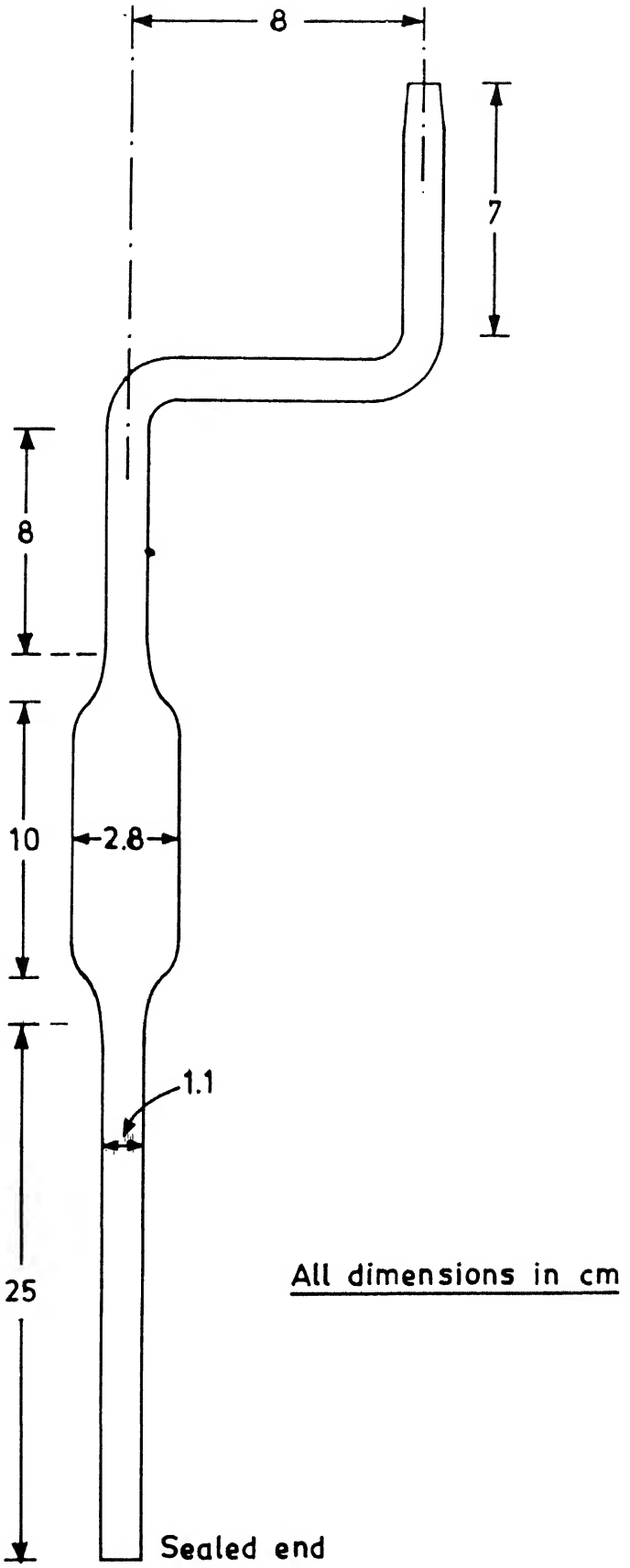

Fig. 2.2. Schematic diagram of specimen capsule.

2.3 Other accessories :

There were a few more accessories which were used through the course of investigation such as slicing holder, argon purification train, cathetometer, stereoscope microscope etc.

2.3.1 Slicing holder :

It was decided to carry out microstructural investigation of the serially sectioned longitudinal specimens of the directionally solidified ingot. Hence it was necessary to part the cylindrical specimen longitudinally into two halves. for this a slicing holder (as shown in Fig. 2.3) was used. It consisted a slot of one millimeter width, which acted as a guide for a manually operated Jeweller's saw while slicing through the specimen.

2.3.2 Argon purification train :

Care was taken for the supply of pure argon which is free of Carbondioxide, Oxygen and moisture in order to maintain an inert atmosphere around the melt. Removal of these impurities was accomplished in a gas purification train. This train consisted of three drying towers, a tube carrying copper turnings and a bubble indicator, all being connected with the commercial argon cylinder in series. Fig. 2.4 gives a schematic view of this purification train. The first drying tower consisting anhydrous calcium chloride and the second one consisting silica-gel are meant for removing moisture. the next tower contains Ascarite where any traces of Carbondioxide are

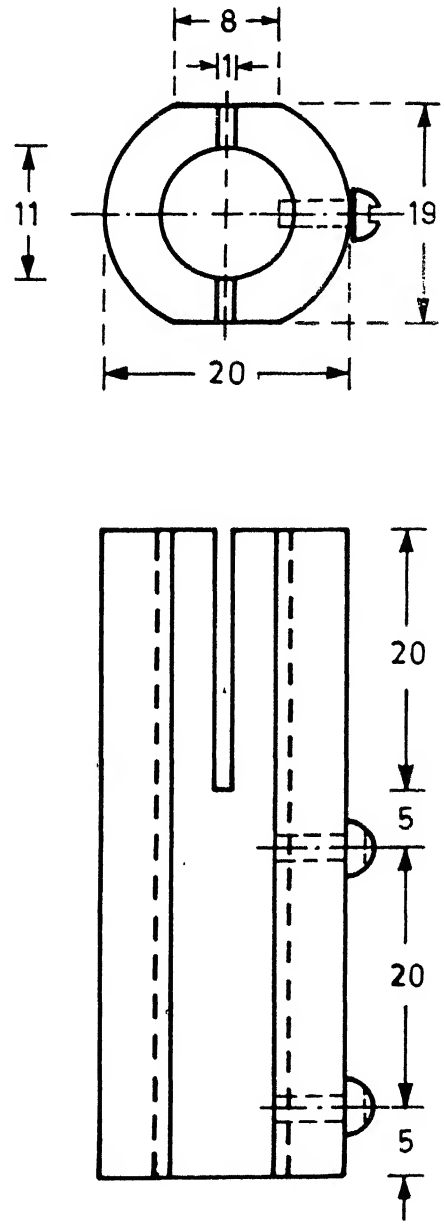

All dimensions in mm

Fig. 2.3. Schematic diagram of slicing holder.

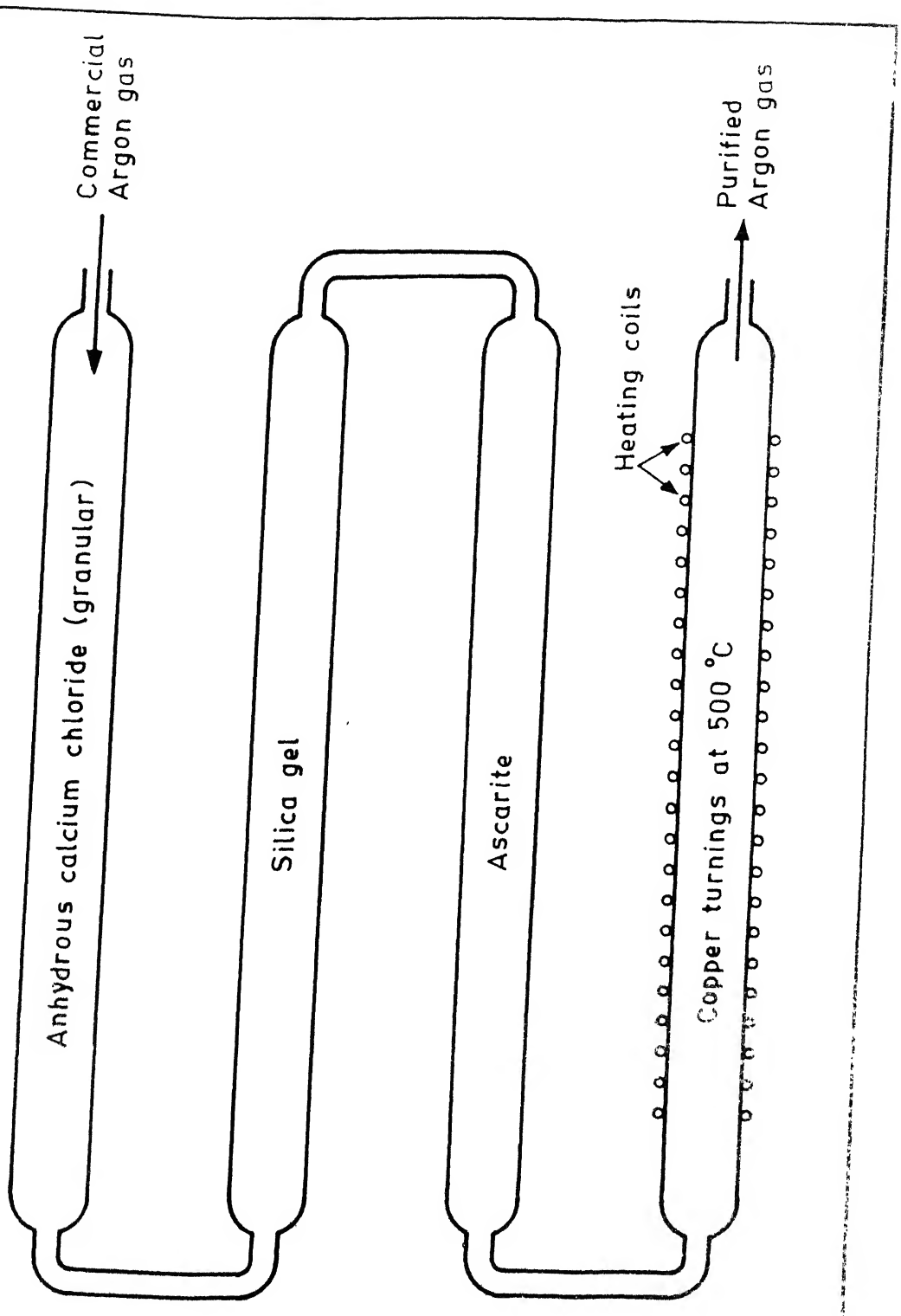

Fig. 2.4. Schematic diagram of argon purification train.

removed. Copper turnings were maintained at 500°c so that any trace of oxygen in the gas would be removed as the argon flowed through it. The clean gas was cooled in a condenser and fed into the solidification unit through the bubble indicator. This indicator was filled with dibutyl phthalate. Number of bubbles coming out of this bubbler per unit time used to give a fair idea about the flow rate of argon gas.

2.3.3 Microscope :

A Nikon stereoscopic microscope SMz-10 was used for detailed morphological observation and their photography. It is specially used for low magnification studies.

Dendrite spacings were measured directly under a binocular microscope with the help of a micrometric eye piece. The micrometric value of this eye piece is defined as the shifting of its index mark by one division of the measuring drum graduation i.e. the circular scale. For a 4x objective this micrometric value was calculated with the help of a stage micrometer scale as follows :

Length to be measured under the objective

$$= a_1 = 100\ \mu m$$

Circular scale reading = a_2 = 93 divisions

$$\therefore \text{Micrometric value} = Y = \frac{a_1}{a_2} = \frac{100}{93} = 1.0753\ \mu m$$

CHAPTER 3

EXPERIMENTAL PROCEDURE

The objective of the present work was to study the manner in which the Primary dendrite arm spacing changes with sudden changes in growth velocities, in directionally solidified Sn-Bi alloys. Hence, the experiment was carried out in three stages :

1) Directional solidification

2) Metallographic specimen preparation

3) Dendrite arm spacing measurements

3.1 Directional solidification :

The crucible carrying the solidified ingot was mounted on its stand and the stand in turn was fixed to the cast iron block (as shown in Fig. 2.1). The furnace was brought down to the lowest possible position. Alignment of the crucible with furnace axis was achieved as far as possible through visual observation and by shifting the cast iron block. The power switch was turned on for the furnace to heat it up. Argon gas was made to flow into the furnace through the purifying train before the alloy would melt. The flow was maintained around 200 bubbles per minute which was considered sufficient to prevent the alloy from oxidation. The chill water was also turned on and its flow was maintained at 300 CC/minute. Gradually the furnace picked up temperature and the ingot started melting from the top towards the chill end. Finally a state of equilibrium was reached when the rate of heat input to the melt was equal to

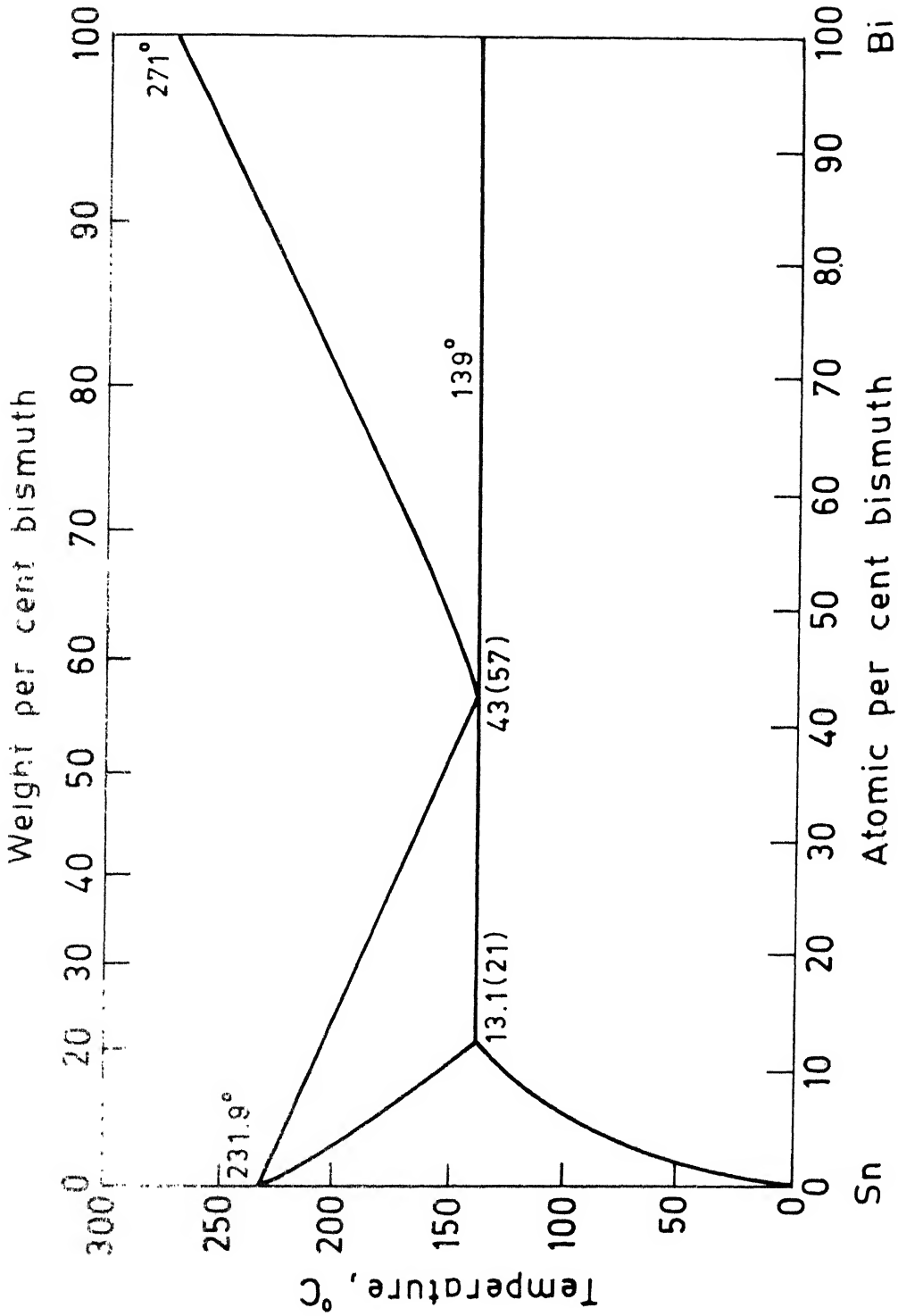

Fig. 3.1. Bi-Sn equilibrium diagram.

the rate of extraction of heat by the chill water and the ingot stand and thus keeping the solid-liquid interface in a dynamic equilibrium. This was confirmed with the help of the measuring thermocouple sheath. This sheath was inserted into the melt (Fig. 2.1) so as to touch the solid-liquid interface. The unchanged reading of the thermocouple top in the cathetometer and the unaltered emf of the thermocouple tip in the potentiometer ensured that the equilibrium had been attained.

The initial interface position in the specimen was deduced from the difference between the cathetometer reading at the top of the thermocouple sheath and its length as explained in Appendix 1. Temperatures at various heights above the solid-liquid interface were measured by raising the thermocouple sheath up. The temperature gradient existing in front of the interface was determined from the plot of these temperatures recorded (given in Appendix 2) versus the distance from the interface (shown in Figures 3.2, 3.3, 3.4, 3.5). The gradients obtained were found to be of the order of 13-14^{o}c/mm. Efforts were made in each of the runs to reproduce this temperature gradient as close as possible by adjusting the temperature controller. The bottom tip of the thermocouple sheath was placed a few (3 to 4) millimeters above the interface during a run and its temperature was noted. The initial position of the index mark on the furnace was also noted (as given in Appendix 3) in the cathetometer. Desired growth rate was set in the speed control potentiometer of the motor and finally the motor switch was turned on for the directional solidification to start. The

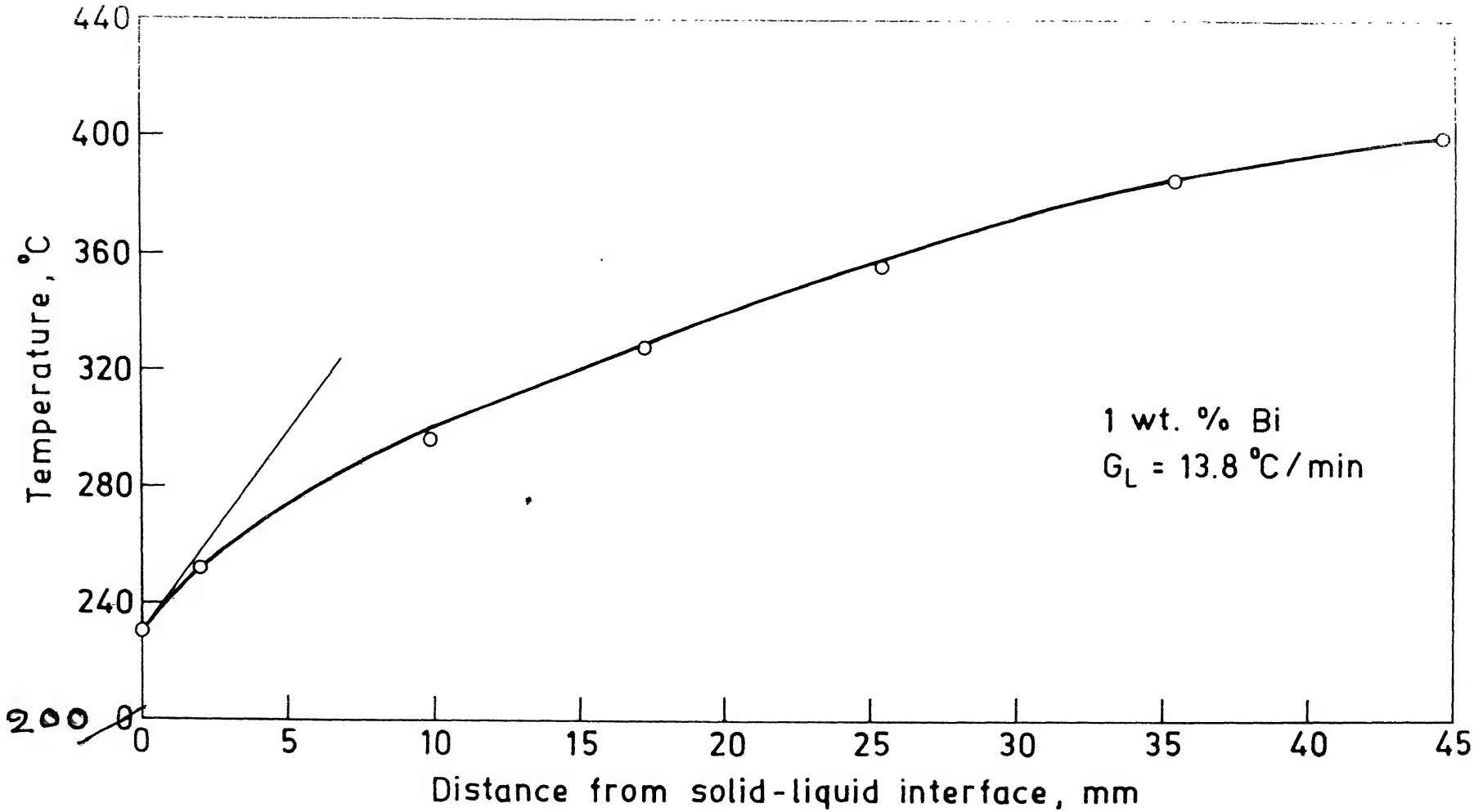

Fig. 3.2. Temperature profile near the solid-liquid interface in run 1 (1 wt. % Bi).

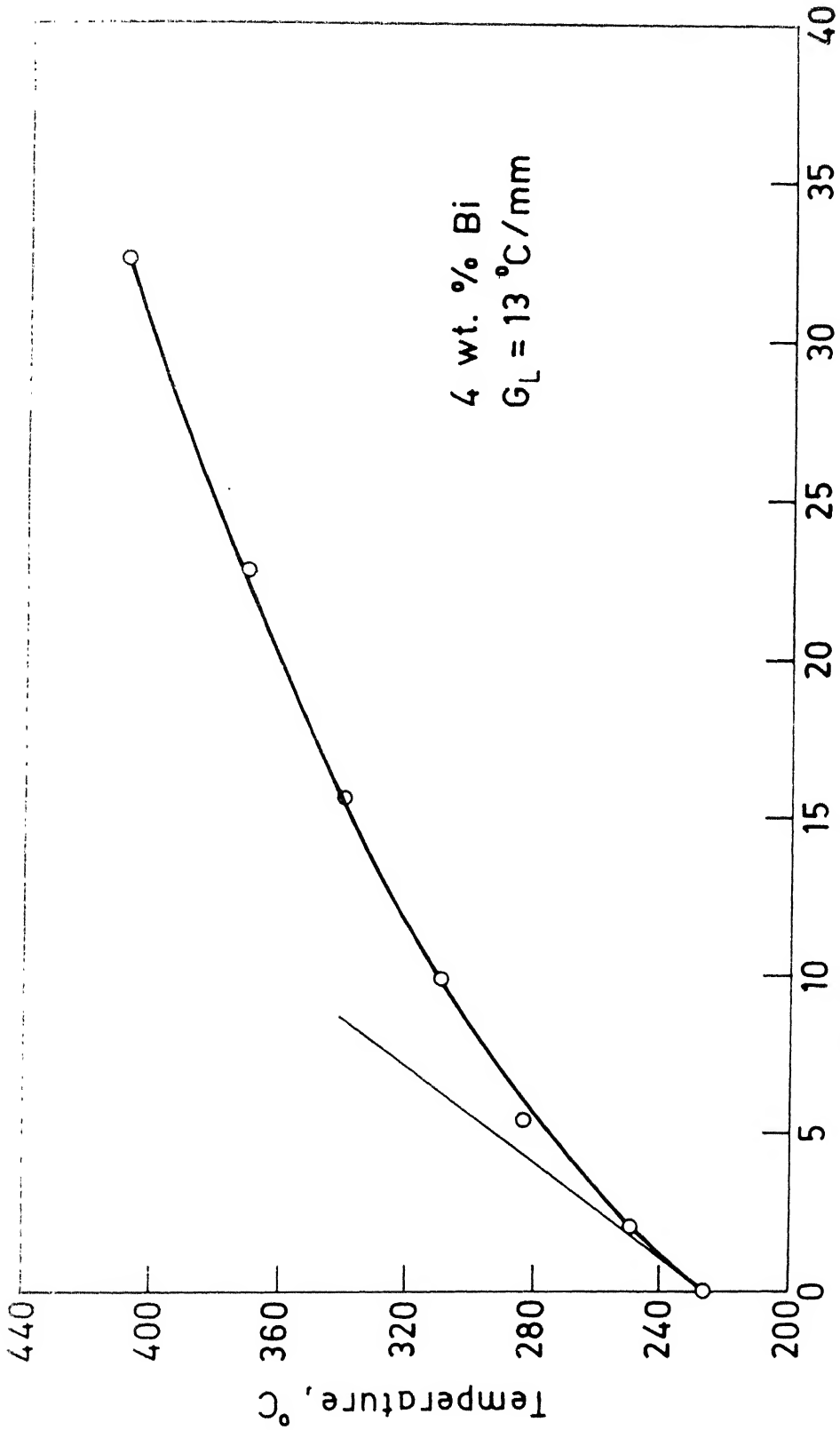

Fig. 3.3. Temperature profile near the solid liquid interface in run 2 (4 wt. % Bi).

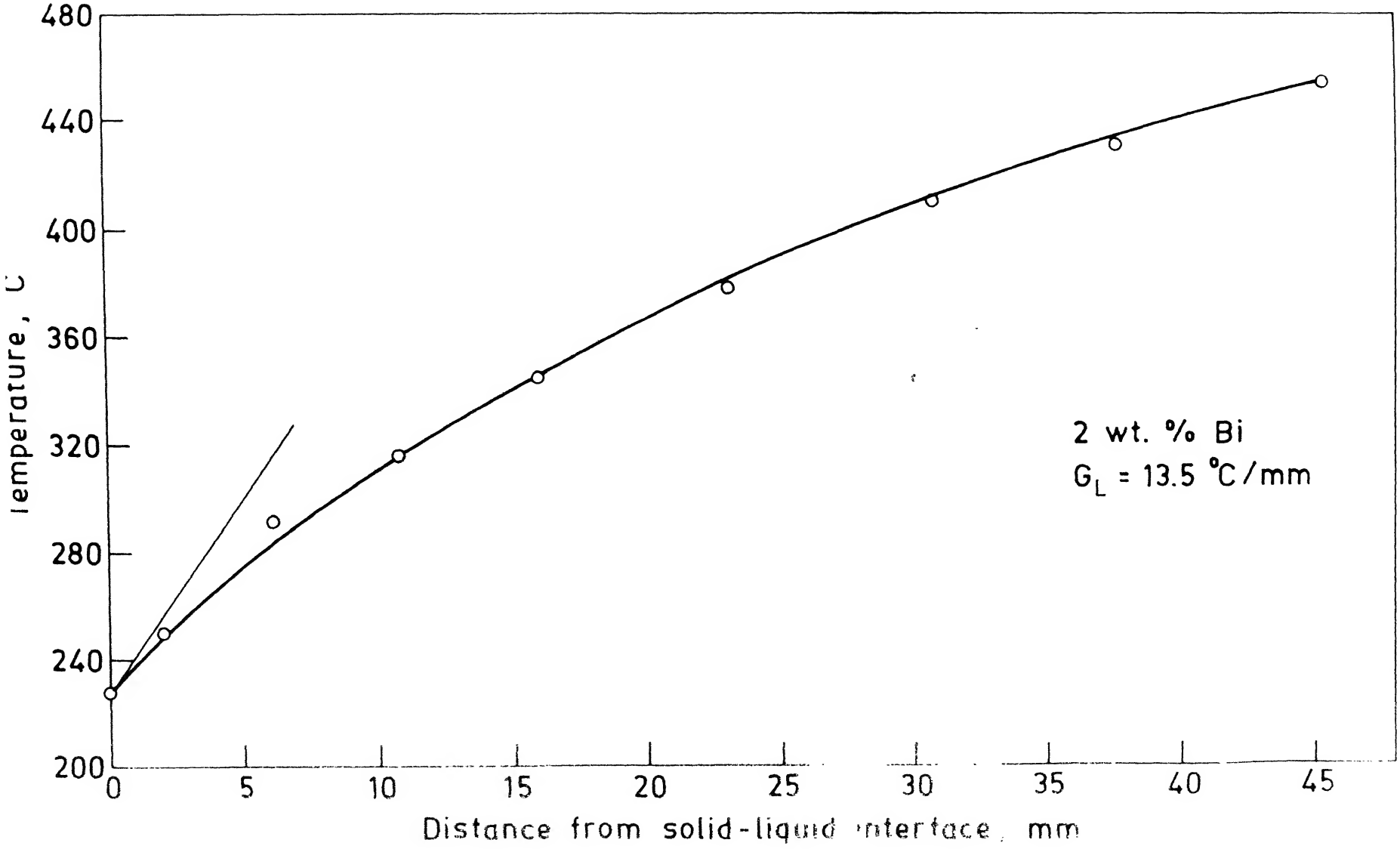

Fig 3.4 Temperature profile near the solid - liquid interface in run 3 (2 wt %

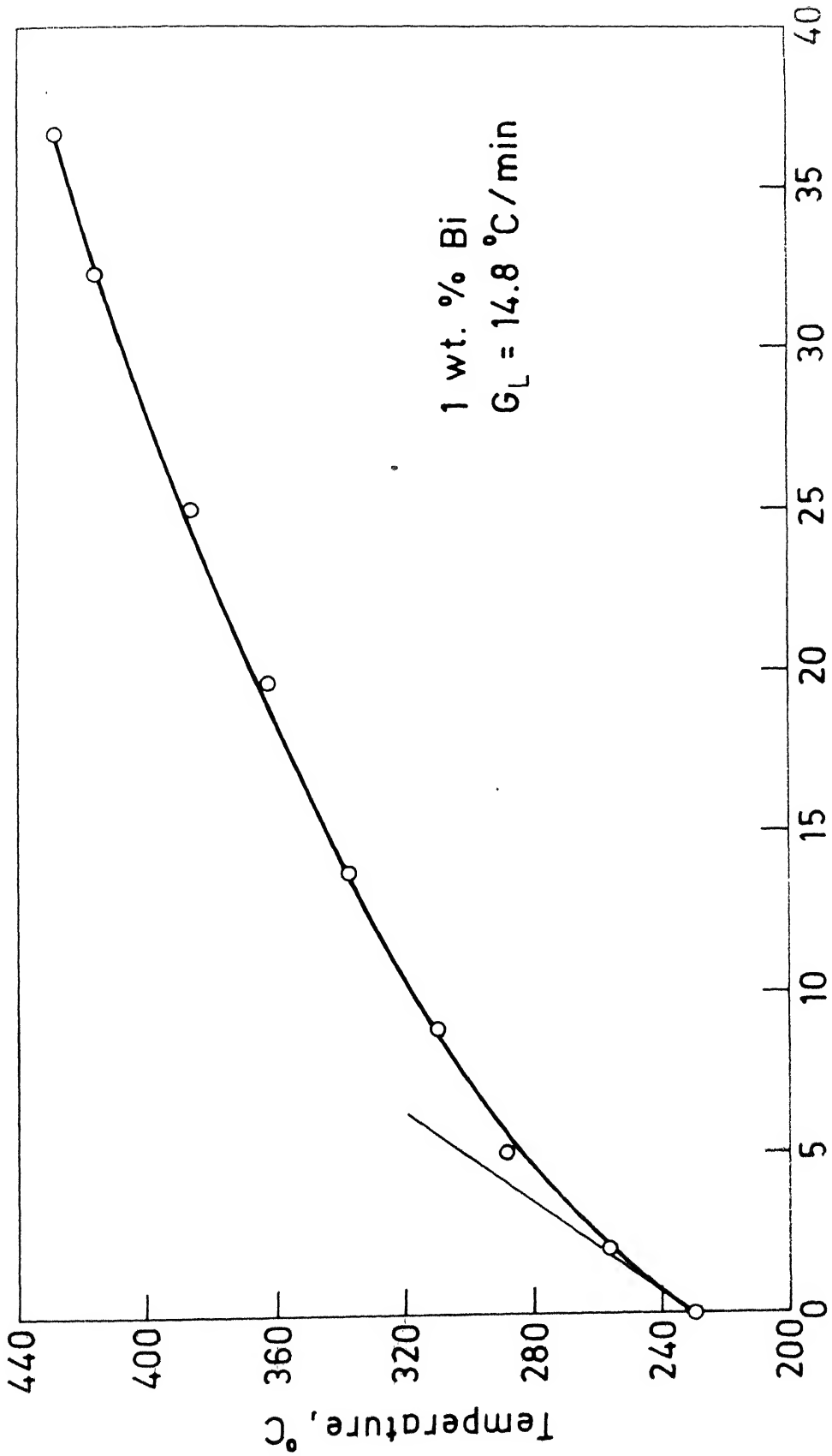

Fig. 3.5. Temperature profile near the solid-liquid interface in run 4 (1 wt % Bi)

temperature of the thermocouple tip was checked frequently during the execution of the run. The furnace was brought to a halt whenever this temperature had either gone down or jumped up much above its initial value, indicating the solid-liquid interface to be too close or too far from the thermocouple tip respectively. This case not at all arised in any of the four runs executed. After a desired length had solidified at the pre-set growth rate, the speed of the motor was changed suddenly to a new value by changing the potentiometer setting of the motor assembly from one setting to another. The change was carried out in less than a second and hence the change in growth velocities from one value to another was assumed to be instantaneous. The actual speed with which the furnace was moving was calculated from the cathetometer readings taken during different rates of freezing. This was done by tracking the index mark on the furnace through the telescopic sight of the cathetometer and noting down the time taken by the furnace to travel that distance with the help of a stop watch. After a successful run, the argon and power supply to the furnace and the water supply to the chill device were stopped. The crucible was carefully withdrawn from the furnace and then broken in order to recover the directionally solidified ingot. The record of cathetometer readings and times are given in tables A.5 to A.8 (Appendix 3).

3.2 Metallographic Specimen Preparation :

The directionally solidified ingot was subjected to preliminary preparations for metallography such as sectioning, mounting, grinding, polishing and finally

appropriate etching so as to reveal the dendritic structure.

3.2.1 Slicing :

The ingot was held securely in the slicing holder (Fig. 2.3) by the two set screws. It was sliced into two longitudinal sections by sawing gently with a thin jewellers saw. This was guided by the diametric slot in the slicing holder so as to move along a single plane of section. One of the sections was further cut into pieces of 2 to 4 centimeters length to get longitudinal sections at various distances from the chill end. Care was taken so as to preserve the initial solid-liquid interface and the interface, at which growth velocity was changed, within one or the other specimen.

3.2.2 Mounting :

Each of these pieces has been mounted on a cold setting mounting material. The mounting material was powdered resin which was made into a thin paste by using an equal volume of hardener (organic solvent). The longitudinal section of each sample was ground to a reasonably flat face before being kept inside the cavity of the metallic mold for mounting. The thin paste of resin was poured over the sample to fill the cavity and kept under a heavy lid. After nearly twenty minutes the resin paste had polymerized into a hard mass and thereby holding the sample in place. All the faces of the cavity in the metallic mold had been greased well, before every mounting for easy removal of the mounted samples. The specimen number and the direction of solidification were marked on each mounted sample for

identification.

3.2.3 Grinding and Polishing :

Initially, each of the mounted samples was given a rough grinding on a flat belt grinder. The transverse section on the top of each longitudinal section was chosen for grinding and polishing and thus on each sample both of these sections were prepared. care was taken to maintain the longitudinal and transverse sections fairly orthogonal to each other. Any sharp edge or extension of the mounting material has been smoothed out during belt grinding. Then every sample was subjected to emery paper polishing. Application of pressure was avoided in order to preserve the solidification structure which would otherwise be lost by surface recrystallization due to heat of friction. Polishing on emery papers was done only along one stroke in a sequential order from coarse to finer i.e., 1/0 to 4/0 size. The direction of polish was changed through 90 degree while going for next finer emery paper. Final polishing was obtained by disk polishing with fine MgO suspension (OP-S suspension of struers) on a polishing cloth. The scratch free polished samples were cleaned thoroughly first with tap water followed by distilled water. The clean specimens were then subjected to etching.

3.2.4 Etching :

The etchant which was used successfully for etching the samples was of the following composition :

Potassium dichromate	:	1 gram
Concentrated hydrochloric acid	:	6 to 8 c.c.
Distilled water	:	86 c.c.

Etching was found to be more efficient if the etchant was poured on to the specimen so as to gently flow over the polished surfaces instead of just dipping the specimen into the etchant. A batch of etchant was used for etching 3-4 samples before being discarded. The etched specimens were cleaned off of the etchant first with tap water and then with distilled water. A little methanol was squirted on the specimen and then it was dried by the blower.

The technique of alternate polishing and etching very frequently has proved advantageous.

3.3 Dendrite Arm Spacing Measurements :

3.3.1 Optical Microscopy :

The specimen so prepared was mounted on a glass slide with plasticene with the help of a specimen mounting press so that the surface under observation remained parallel to the focal plane of the microscope. Both the sections i.e. longitudinal as well as transverse of a specimen were critically observed at various low magnifications, in a 'Nikon' stereoscopic zoom microscope. Photographs on both the sections were taken. These photographs were taken (1) on the longitudinal sections in the regions where a change in the growth rate had been made and (2) on both the longitudinal and transverse sections near their common edge so as to measure angles made by the primary dendrite

platelets with the edge. The figures 3.6, 3.7, 3.8, 3.9, 3.10, 3.11, and 3.12 show these photographs.

3.2.2 Measurement of Primary Dendrite Spacings :

While preparing the samples care was taken so that the transverse sections were perpendicular to the longitudinal sections. If λ is the apparent primary dendrite spacing on the longitudinal section which is measured along a direction normal to the platelike dendrites, then λ_o the true spacing is given as

$$\lambda_o = \lambda K \qquad (1)$$

where

$$K = \frac{\sin \theta_b}{(1-\cos^2\theta_a \cos^2\theta_b)^{1/2}} \quad . \qquad (2)$$

where θ_b = The angle made by the platelike dendrites with the edge of the transverse section.

and θ_a = The angle made by dendrites with the edge of the longitudinal section.

This formula was modified and adopted from the original one proposed by V. Bansal[14] which is applicable for measurements on transverse sections (as explained in Appendix 4).

Apparent primary dendrite spacing measurements were carried out with the help of a micrometric eyepiece fitted to one of the eyepiece tubes of a binocular microscope (model 'CENSICO'). The specimen was aligned parallel to the edge of the glass slide prior to pressing. The binocular microscope consists of two stage verniers. The specimen was aligned

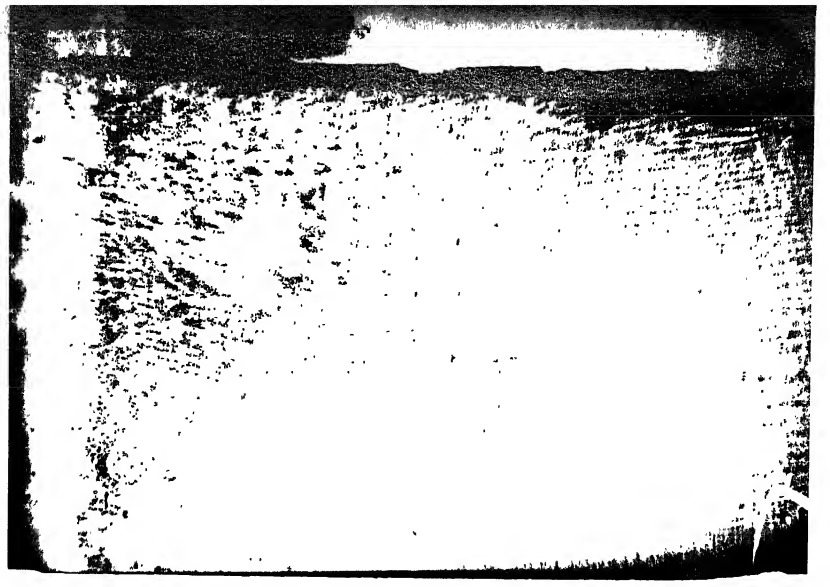

Fig. 3.6 The start of directional solidification in ingot 2 (4wt% Bi in Sn). Sample 22. Mag = 10.15×

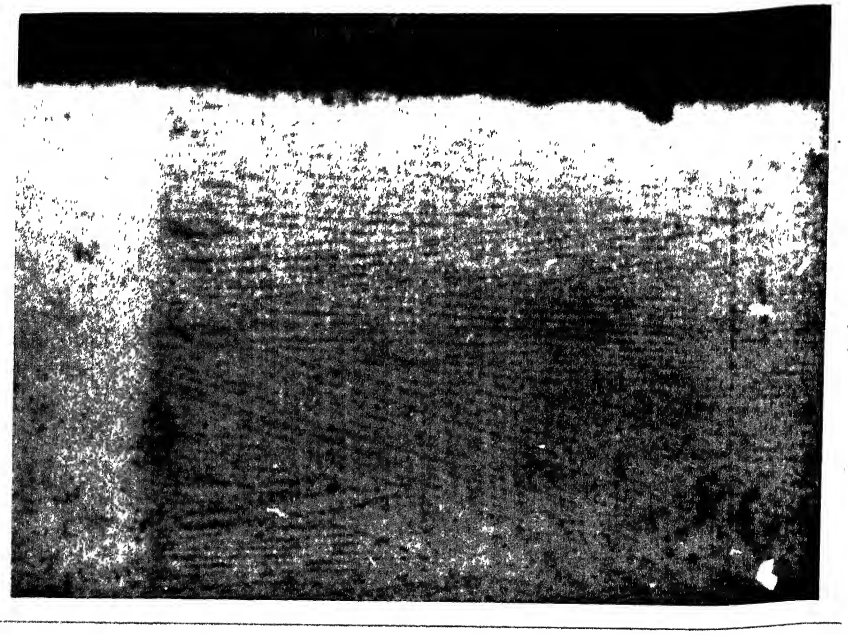

Fig 3.7 The start of directional solidification in ingot 3 (2wt% Bi in Sn). Sample 32. Mag = 10.15×

Fig 3.8 Shows the immediate increase in P.D.S. due to the infinite deceleration in freezing rate (-7.91) in ingot 2 (4wt% Bi in Sn) sample 24. Mag = 10.15x

Fig 3.9 Shows the immediate decrease in P.D.S. due to the infinite acceleration in freezing rate (10.71) in ingot 2 (4wt% Bi in Sn) sample 24. Mag = 10.15x

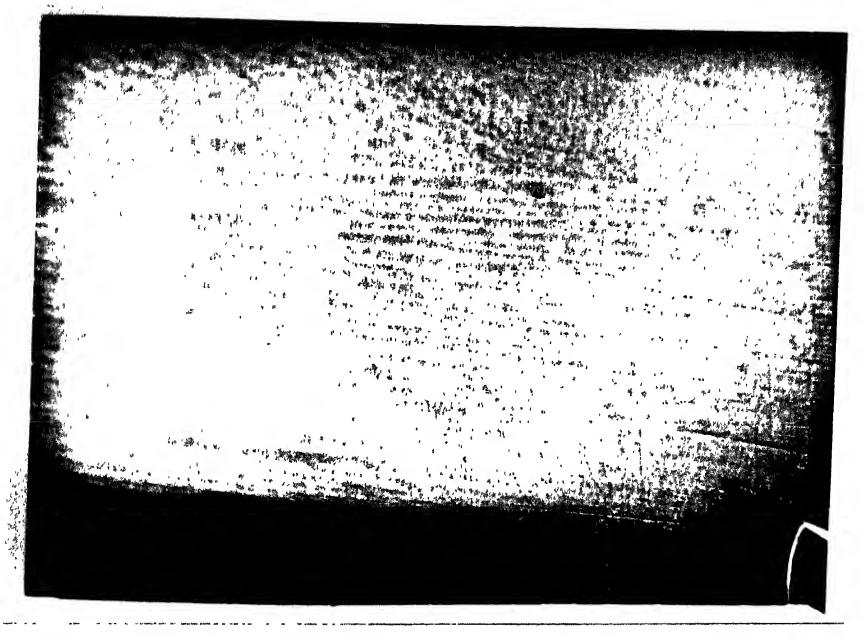

Fig 3.10 Shows the immediate decrease in P.D.S. due to the infinite acceleration in freezing rate (10.71) in ingot 2 (4wt% Bi in Sn) sample 26. Mag = 14.29x

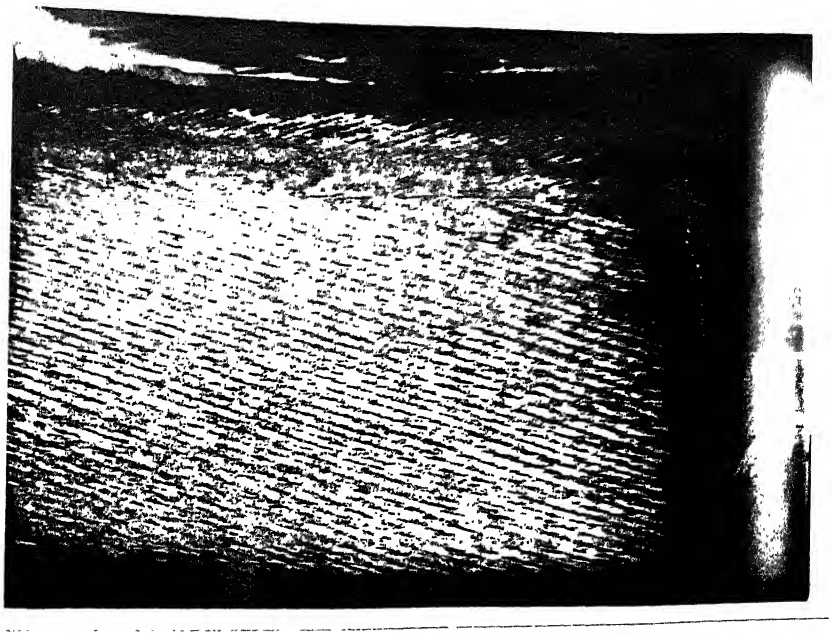

Fig. 3.11 Shows the longitudinal edge of sample 34 (ingot 3, 2wt% Bi in Sn) $\theta_a = 74^o$. Mag. = 10.15×

Fig. 3.12 Shows the corresponding transverse edge of sample 34 (ingot 3, 2wt% Bi in Sn) $\theta_b = 41.5^o$. Mag. = 14.29×

along one of the verniers and keeping the other vernier fixed. Each longitudinal specimen was observed first in the `Nikon' stereoscopic microscope and the grain along which the P.D.S. measurements were to be taken was selected and the selected grain should be such that it can be clearly followed from the bottom of the specimen to its top. All spacing measurements were taken on the longitudinal specimens. The grain selected for measurements should have a clear intercept on the transverse sections.

The bottom of each specimen was noted from the stage vernier and then this vernier was moved from the bottom to the top roughly by one millimeter in each step. The micrometric eyepiece measurements were recorded and also the no of dendrites in that distance at each step. These readings are presented in a tabular form in Appendix 5.

3.3.3 Angle Measurements :

The grains along which the measurements were made were photographed at the common edge on both the longitudinal and transverse sections. A line is drawn along the edge and another line is drawn which is parallel to the platelike dendrites. The acute angles were measured directly on the photographs. These angle measurement data is presented in tabular form in Appendix 6. These angles are required to calculate `K' from the equation (2) to get true lamellar spacing.

CHAPTER : 4

RESULTS AND DISCUSSION

The directionally solidified ingots were subjected to metallographic investigation in order to determine the primary dendrite spacing. The individual primary dendrites are lamellar and grow approximately along the heat flow direction. A grain consists of several such lamellae stacked parallel to each other.

4.1 Primary Dendrite Spacing :

The distance between the centers of two adjacent plates has been measured as the primary dendrite spacing (PDS) in the present work. Measurements of PDS have been carried out throughout the length of each ingot. The real PDS data on each ingot are presented in tables 9, 10, 11 and 12 in Appendix : 5.

4.2 Manner of change in PDS :

The primary dendrite spacing measurement on each ingot has been ploted (Figures 4.1, 4.2, 4.3 and 4.4) with PDS values on Y-axis and Distance from the starting interface on X-axis. The sketch of each ingot has also been drawn on the respective plots. At each observed change in freezing rate as indicated by a sudden and drastic change in PDS, a vertical line has been drawn. Downward arrow mark (↓) on the X-axis indicates the position where a change in freezing rate was made calculated from cathetometer measurements of the movement of the furnace. In these runs the steady state freezing rate was either 1) abruptly increased i.e. infinitely rapid acceleration or 2) abruptly decreased i.e. infinitely rapid deceleration. On graphs (figures 4.1 to 4.4) an

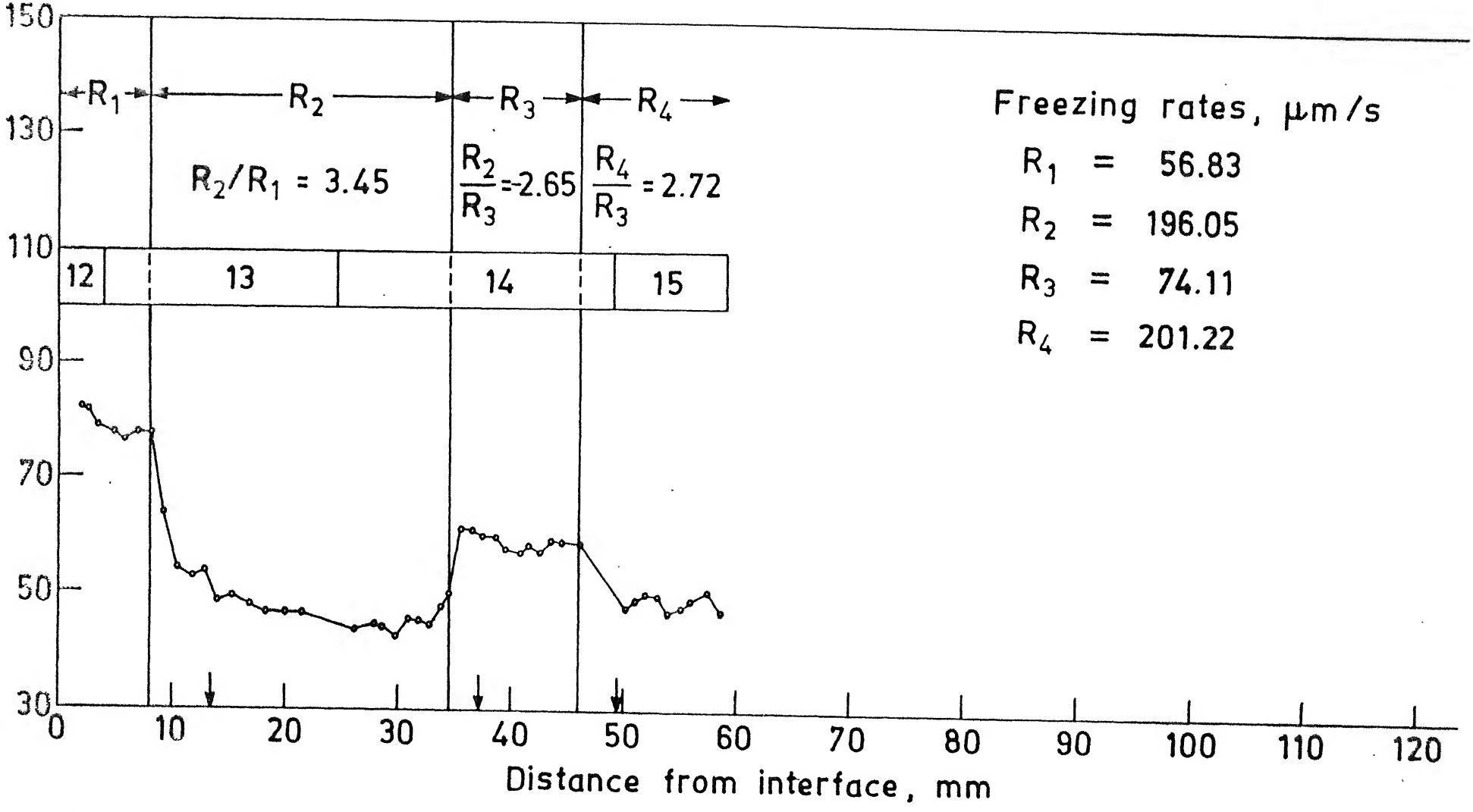

Fig. 4.1. Primary dendrite spacing (P.D.S.) vs. distance from the start of directional solidification for ingot no. 1 (1 wt. % Bi in Sn).

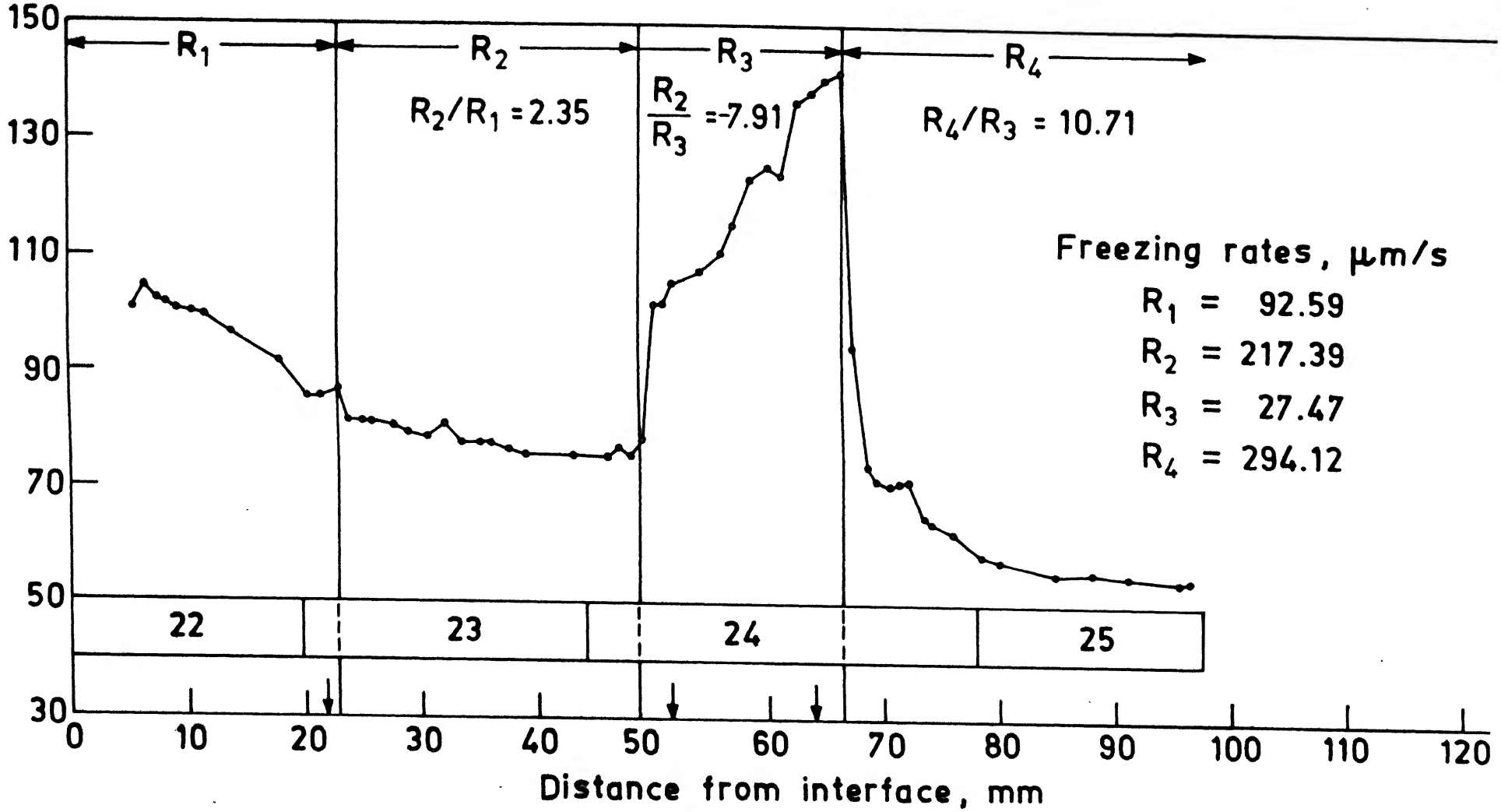

Fig. 4.2. Primary dendrite spacing (P.D.S.) vs. distance from the start of directional solidification for ingot no. 2 (4 wt. % Bi in Sn).

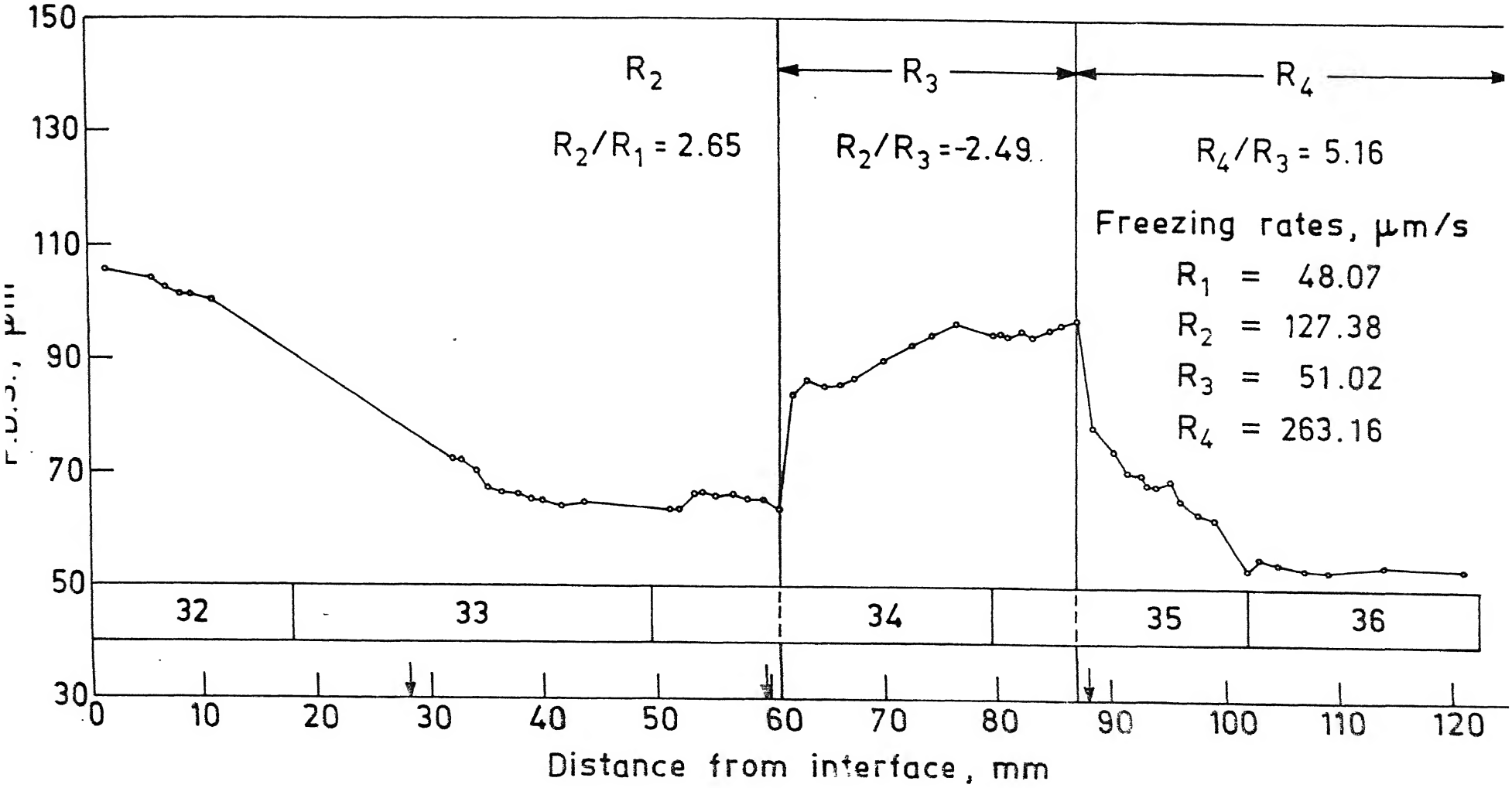

Fig. 4.3. Primary dendrite spacing (P.D.S.) vs. distance from the start of directional solidification for ingot no. 3 (2 wt. % Bi in Sn).

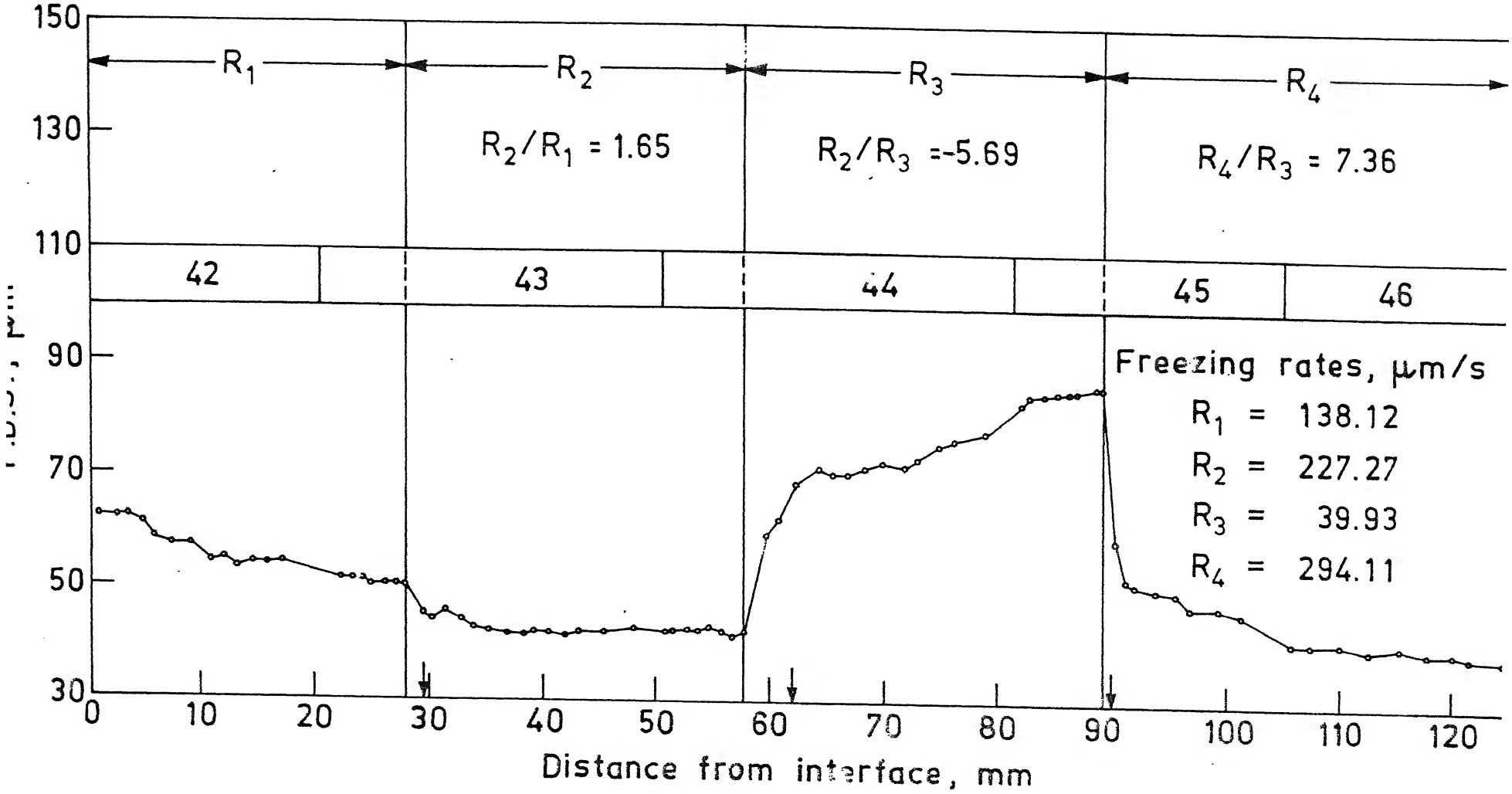

Fig. 4.4. Primary dendrite spacing (P.D.S.) vs. distance from the start of directional solidification for ingot no. 4 (1 wt. % Bi in Sn).

abrupt decdrease in freezing rate has been represented by putting negative (-) sign in front of the value of the RHIGH/RLOW ratio.

In all of these graphs (figures 4.1 to 4.4) one observes that the dendrite spacing responded immediately to the change in freezing rates (either infinite acceleration or deceleration) over a short distance of the order of 1 to 2 mm from the point where a change in freezing rate was made. The change in spacing continues but more gradualy, and finally reaches a new steady state value over distances which are in the range of 10 to 25 mm. In figure 4.3 the change in freezing rate from 48.07 μm/S to 127.38 μm/S (infinite acceleration) could not be determined since a suitable grain was not available on the longitudinal section of the sample, which ran through its entire length which is necessary in the present scheme of PDS.

This observation of an immediate change in inter lamellar spacing to the new value upon an abrupt increase in freezing rate, has also been reported by Hiller and Rau[15] in cutectic iron alloys and by Mollard and Flemings in Pb-Sn System.

4.3 Immediate adjustment in Spacings :

The response in adjustment of primary dendrite spacing is more immediate initially over a distance of 1 to 2 mm from position where the freezing rate change was imposed (either infinite acceleration as deceleration) and its found gradual after this immediate adjustment. This immediate adjustment data is presented in a tabular form in Table 4.1.

This table gives the ratio of freezing rate change imposed (RHIGH/RLOW), the distance in mm over which the immediate change has occured and the time taken for this adjustment

Table 4.1

Immediate adjustment in spacings

ingot no (wt% Bi)	Ratio of freezing rate change imposed RHIGH/RLOW		Distance in mm over which the spacing changed abruptly	Time taken for immediate adjustmentin in seconds	% adjustment immediately P.D.S.
1 (1wt%Bi)	$\frac{196.05}{56.83}$	= +3.45	2.25	11.48	75.86
2. (4wt% Bi)	$\frac{217.39}{92.59}$	= +2.35	1	4.6	45.83
	$\frac{217.39}{27.47}$	= -7.91	1.25	45.5	40.91
	$\frac{294.12}{27.47}$	= +10.71	2	6.79	79.07
3. (2wt% Bi)	$\frac{127.48}{51.02}$	= -2.49	1.25	24.5	58.62
	$\frac{263.16}{51.02}$	= +5.16	1.5	5.69	42.86
4. (1wt% Bi)	$\frac{227.27}{39.93}$	= +1.65	1.5	6.6	64.28
	$\frac{294.11}{39.13}$	= -5.69	1.75	43.83	39.29
		+7.36	1.5	5.1	73.93

(calculation based upon the new freezing rate) and the immediate percentage adjustment in the PDS which was calculated on the basis of the total difference in the steady state P.D.S. values before and after the change in freezing rate.

From the table 4.1 it appears that the extent of immediate adjustment in spacing is more greater percentage adjustment accomplished in case of rapid accelerations as compared to rapid decelerations (represented by negative sign). This it is seen that in the case of abrupt aceelerations, the extent of the immediate adjustment range from 43 to 79 poercent while for abrupt deceleration the range is 39 to 59 percent. Here the term immediate adjustment is defined as the adjustment in primary dendrite spacing that has taken place over a short distances (from the point of imposed change in freezing rate).

The difference in the immediate adjustment for acceleration and decelerations is more striking when the time taken for the same are compared. It is again seen from table 4.1 that in the case of abrupt accelerations, the time taken for `immediate adjustment' ranges from 4.6 to 11.5 seconds while the corresponding range for the abrupt deceleration is 24.5 to 45.5 seconds.

4.4 Total readjustment in spacings to the new values :

When a freezing rate change was imposed it is found that the change in primary dendrite spacing is more drastic over a distance of the order of 1 to 2 mm and is gradual beyond that till it reaches a new steady state value corresponding to the new freezing rate. This data of the total time taken by the PDS to reach the new steady state value and the distance and time over

Table 4.2

Total readjustment in spacings to the new values

ingot no	Ratio of freezing rate change imposed RHIGH/RLOW	Distance in mm over which the spacing has adjusted	Time taken in seconds for adjustment
1 (1wt% Bi)	+3.45 = 196.05/56.83	7	35.71
	-2.65 = 196.05/74.11	9	121.44
	+2.72 = 201.22/74.11	10.5	52.18
2 (4wt% Bi)	+2.35 = 217.39/92.59	16	73.6
	-7.91 = 217.39/27.47	16	582
	+10.71= 294.12/27.47	18.5	62.89
3 (2wt% Bi)	-2.49 = 127.48/51.02	15.5	303.8
	+5.16 = 263.16/51.02	15.5	58.89
4 (1wt% Bi)	+1.65 = 227.27/138.12	20	88
	-5.69 = 227.27/39.93	25	626
	+7.36 = 244.11/39.93	16.5	56.1

which it has adjusted to the new steady state value are presented in tabular form in Table 4.2.

From the Table 4.2 it is observed that the time taken for adjustment is more in case of abrupt decelerations as compared to abrupt accelerations. It's interesting to note that in a given ingot, the distance over which the adjustment is completed is roughly of the same irrespective of the change in freezing rate being either infinite acceleration or infinite deceleration and irrespective of the amount of change made in the freezing rate. In case of ingot : 1, this distance is 7 to 10 mm, in ingot : 2 this is 16 to 18.5 mm, in ingot : 3 it is 15.5 mm and in ingot : 4 it is 16.5 to 25 mm. However the difference in the time taken for the attainment of the new steady state PDS in the case oc acceleration and deceleration are enourmous. From table 4.2 it is seen that the total times in the case of accelerations range from 35.7 to 88 seconds while from deceleration they range from 121.4 to 626 seconds.

It is seen from tables 4.1 and 4.2 that the concerntration of solute (bismuth) has no marked influence over either the distance or time taken for the immediate or final adjustment in PDS.

Neff et al.[17] report that the adjustment to new spacing was gdradual for decelerations but was instantaneous for accelerations. Neff[17] also observed microstructurally that lamellar branching is significantly easier to accomplish than lamellar termination. This could be one reason why lowering of PDS (by branching) could be accomplished faster for accelerations compared to an increase in PDS (requiring lamellar terminations) for decelarations.

4.5 Plot of Steady State P.D.S vs Freezing rate :

The steady state primary dendrite spacing value for each freezing is given in tabular form in table 4.3. These values are then plotted in Fig. 4.5 on a long-log graph. The data points exhibited a linear fit with negative slopes of 0.396 in case of ingot 1 and 4, (1 ωt% Bi), 0.395 incase of ingot 3 (2ωt% Bi) and 0.448 in case of ingot :2 (4 ωt % Bi). Das has reported a value of 0.36.

A Log-Log graph of PDS Vs composition is also plotted and shown in Fig 4.5. The positive slopes of 0.409, 0.387 and 0.425 respectively.

Table 4.3

Steady state P.D.S values and the freezing rates

Ingot No.	Freezing rate in μm/S	Steady rate P.D.S in μm
1	56.83	76
	75.11	60
	196.05	47
	201.22	46
2	27.47	141
	92.59	87
	217.39	75
	294.12	55
3	48.07	100
	51.02	96
	127.38	67
	263.16	54
4	39.93	85
	138.12	50
	227.27	43
	294.11	40

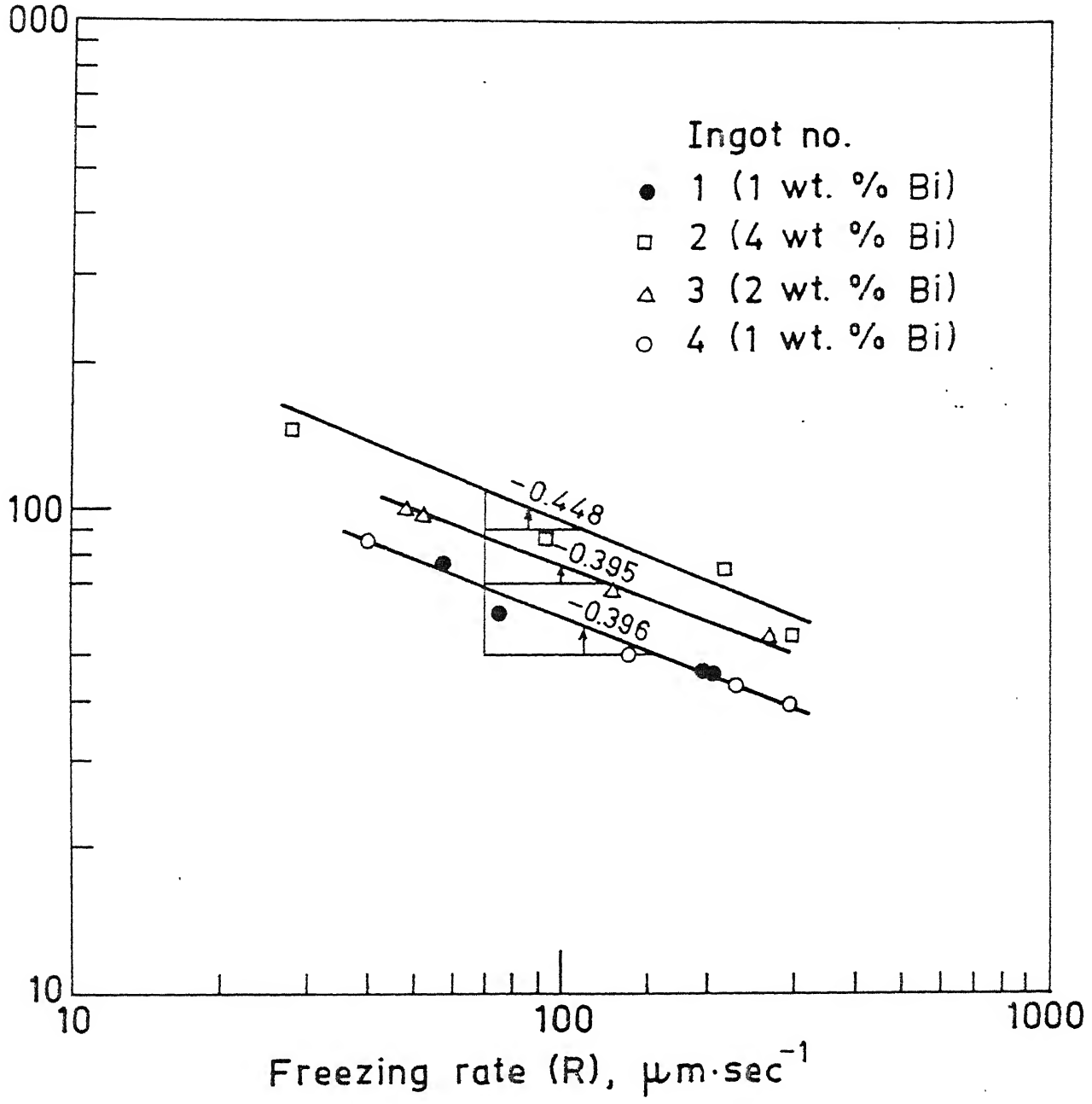

Fig. 4.5. Variation of P.D.S. with freezing rate.

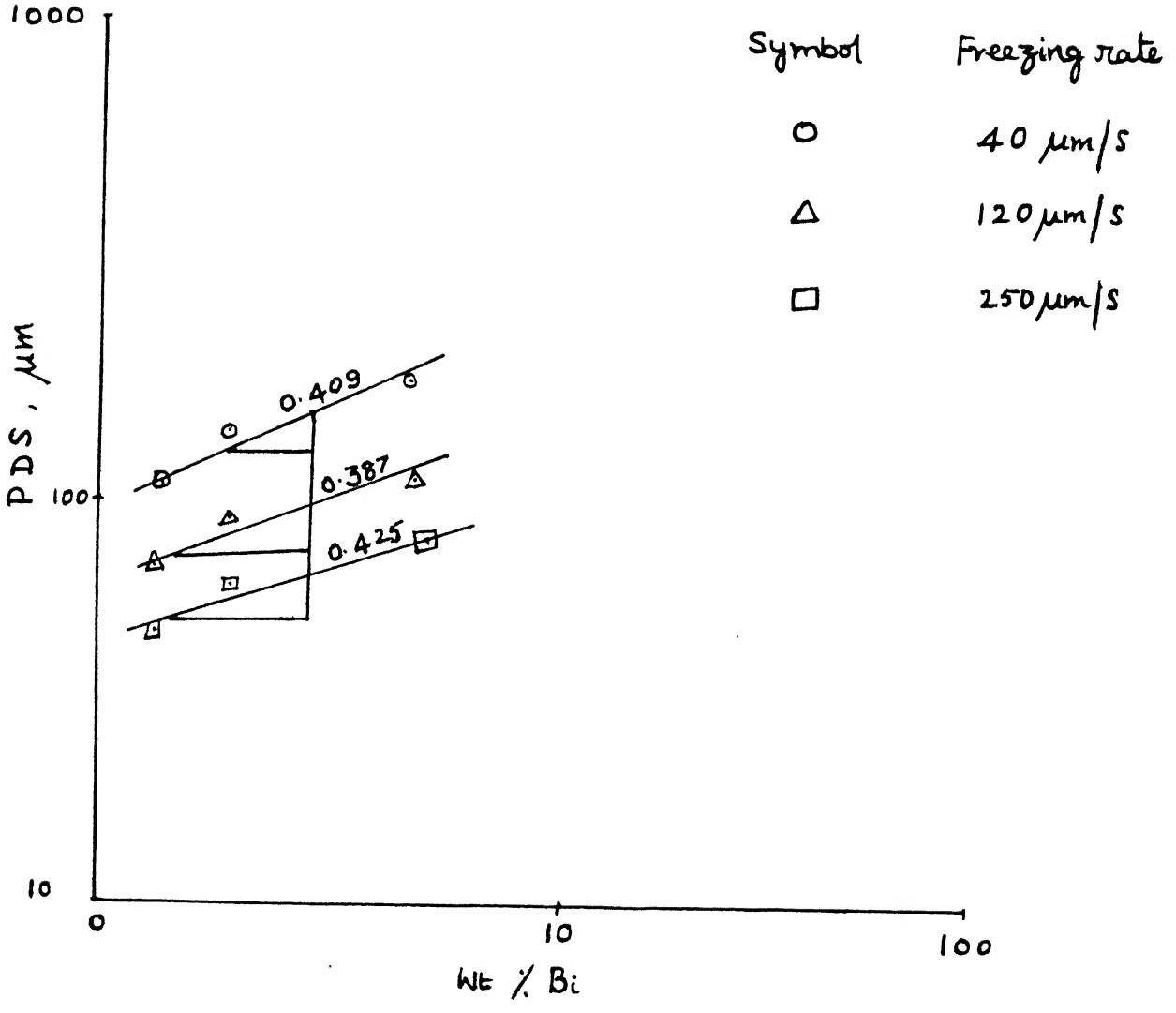

Fig. 4.6 Variation of PDS with Solute Content

CHAPTER : 5

CONCLUDING REMARKS

5.1 CONCLUSIONS

For directionally solidified dilute binary alloys of Bismith (1 to 4 weight percent) in tin it is observed that -

1) When an abrupt change of freezing rate is brought about ranging from +1.65 to 10.71 (acceleration) or -2.49 to -7.91 (deceleration) there is an immediate readjustment in the primary dendrite spacing which occurs over distances of 1 to 2mm.

2. The extent of the immediate readjustment is greater for acceleration than it is for deceleration.

3. The distance over which the new steady state primary dendrite spacing gets established following an abrupt change in freezing rate varies from about 15 to 25 mm and is independent of the fact whether the change is an acceleration or a deceleration.

4. The time taken for immediate as well as total readjustment in the primary dendrite spacing is 4 to 8 times greater for decelerations compared to what it is for accelerations of the freezing rate.

5. The primary dendrite spacing (λ) seems to have the following sample correlation with the concerntration of solute in atom percent (C) and freezing rate (R).

$$\lambda = K C^{l} R^{m}, \text{ where K is a constant.}$$

The value of l is found to vary from 0.387 to 0425 and that of m from -0.395 to -.0448.

5.2 Suggestion for further work

In the present work the maximum RHIGH/RLOW tried was 10.71. This ratio has to be further increased to understand the exact mechanism by which the spacing adjusts. It should be further investigated to explain why in case of infinite deceleration it takes more time for adjustment.

LIST OF REFERENCES

1. Giamel, A.F. and Erickson, I.S., `Super Alloys Metallurgy and Manufacutre' (1966) pp 1-2.
2. Mclean, M., `Directionally Solidified Material for High Temperature Service' Pub. Metals Society (1983).
3. Galasso, F.S., `J. of Metals' (1967), Vol. 19, pp. 17.
4. Chalmers, Bruce, `Principle of Solidification' (1964), pub. John Willey and Sons, pp 201.
5. Tiller, W.A. and Jackson, K.A., `Acta Metallurgiea' (1953), Vol. 1, pp. 428.
6. Zener, C. `Trans. AIME' (1946), Vol. 167, pp. 550-95.
7. Dean, H. et. al. `J. of Crystal Growth' (1974), Vol. 21, pp. 51-57
8. Double, D.D., `Meterials Science and Engg.' (1973), Vol. 11 pp. 325
9. Elliot, R., `Eutectic Solidification processing' (1983), pub. Butterworth and Co. pp. 308.
10. Neff, M.A. and Rickinson, B.A., `Met. Trans.'(1978), Vol. 9B, pp. 469.
11. Rambabu Karlopudi, M. Tech. Thesis (1980), I.I.T. Kanpur.
12. Das Niranjan, M.Tech. Thesis (1984), I.I.T. Kanpur.
13. Kain Vinod Kumar, B.Tech. Thesis (1981), I.I.T. Kanpur.
14. Bansal, V., `J. of Material Science Letters' (1989), Vol.8, pp. 451-52.
15. Hiller, M. and Subba Rau V.V., `Iron and Steel Institute' (1976), Vol. 110, Brighton, England.
16. Mollard, F.R., and Flemmings, M.C. `Trans. AIME' (1967), Vol 239, pp. 1534.
17. Neff, M.A. and Rickinson, B.A., `Met. Trans.' (1978), Vol. 9B, pp. 469.
18. Hunt, J.D., `Proceedings of an International Conference on Solidification, University of Sheffield on 18-21, July 1977, Pub. Metal Society, London (1979), pp. 3-9.

APPENDIX : 1

Determination of the Position of solid-liquid interface

The following method was adopted to precisely determine the Position of the solid-liquid interface with reference to the bottom of the crucible containing the ingot.

As shown in figure 2.1 (Schematic diagram of solidification apparatus), the following fixed distances were measured before the run

Let B = Height of the cork arrangement,

C = Total furnace height,

D = Total thermocouple sheath height,

F = Total height of the crucible stand,

K = Distance from the lower surface of annular ring to the furnace bottom.

After thermocouple is adjusted such that it exactly touches the solid-liquid interface the following variable distances have to be measured after equilibrium is attained in the system.

A = The length of the thermocouple sheath that is visible above the cork arrangement.

H= The initial length of the, crucible stand from the lower surface of the annular ring to the base of the stand.

Let the solid-liquid interface be at any position after equilibrium is attained.

K + H =	Height of the Crucible stand from furnace bottom to the base,
{F-(K+H)}	Height of crucible stand that is projecting inside the furnace.
{D-(A+B)}	Height of thermocouple sheath inside the furnace.

So, $\left[C - [\{D-(A+B)\} + \{F-(K+H)\}]\right]$ gives the exact height of the solid-liquid interface with respect to the bottom of the crucible.

APPENDIX : 2

Distribution of temperature Profile in the melt.

Table :A·1 Run : 1 (ingot : 1 i.e. 1ωt% Bi in Sn)

S.No.	Distance of thermocouple tip from interface in mm	e.m.f. in mV	Temperature with Room Temp correction in ^{o}c
1	2	9.04	252
2	9.87	10.83	297
3	17.21	12.11	328
4	25.39	13.27	356
5	35.42	14.49	385
6	44.57	15.18	400

Table :A·2 Run : 2 (ingot : 2 i.e. 4ωt% Bi in Sn)

S.No.	Distance of thermocouple tip from interface in mm	e.m.f. in mV	Temperature with Room Temp correction in ^{o}c
1	2	8.94	250
2	5.31	10.3	284
3	9.78	11.36	310
4	15.55	12.59	340
5	22.74	13.99	372
6	32.5	15.55	410

Table :A3 Run : 3 (ingot : 3 i.e. 2ωt% Bi in Sn)

S.No.	Distance of thermocouple tip from interface in mm	e.m.f. in mV	Temperature with Room Temp correction in ^{o}c
1	2	8.93	251
2	6.09	10.59	292
3	10.65	11.6	317
4	15.86	12.78	345
5	23.16	14.21	379
6	30.69	15.54	411
7	37.56	16.39	431
8	45.3	17.37	454

Table :A4 Run : 4 (ingot : 4 i.e. 1ωt% Bi in Sn)

S.No.	Distance of thermocouple tip from interface in mm	e.m.f. in mV	Temperature with Room Temp correction in ^{o}c
1	2	9.25	258
2	5.07	10.52	289
3	8.86	11.39	310
4	13.7	12.51	338
5	19.64	13.59	363
6	24.98	14.48	385
7	32.26	15.76	415
8	36.69	16.23	427
9	41.9	16.92	452

APPENDIX : 3

Determination of Freezing rates with which the solid-liquid interface has moved in the runs Performed.

The initial position of the index mark on the furnace was noted down in the cathetometer with the help of the telescopic sight. Then the motor was switched on after setting it at the desired speed. The cathetometer readings are taken during the different rates of freezing. The real time was noted at each reading with the help of the stop watch. Then the freezing rate was suddenly changed and the real time at which the speed change was made was also noted. From these cathetometer readings and the time interval in which these readings are taken the actual freezing rate with which the solid-liquid interface is moving was calculated. Using this actual freezing rate the position of the change in freezing rate was back calculated. The following tables give these calculations on the four runs performed.

Table :A.5 Run : 1 (ingot : 1 i.e. 1ωt% Bi in Sn)

Potentiometer setting	Real time	Time interval	Cathetometer readings in cms	Diff between cathetometer readings in cms	actual freezing rate in μm/s
	0		8.917		
5.19	11.41'52"	142"	9.264	0.807	56.83
	11.44'14"		10.071		
			10.264		
Freezing rate changed at	11.44'48"		(Back calculated)		
5.24	11.45'54"	38"	19.541	0.745	196.05
	11.46'32"		10.071		
Freezing rate changed at	11.46'50"		12.639 (Back calculated)		
5.18	11.48'32"	34"	13.512	0.252	74.11
	11.49'06"		13.764		
Freezing rate changed at	11.49'22"		13.882 (Back calculated)		
5.24	11.50'09"	49"	14.826	0.986	201.22
	11.50'58"		15.812		

Table :A.6 Run : 2 (ingot : 2 i.e. 4ωt% Bi in Sn)

Potentiometer setting	Real time	Time interval	Cathetometer readings in cms	Diff between cathetometer readings in cms	actual freezing rate in μm/s
	0		7.869		
5.205	12.0' 55"	2'42"	8	1.5	92.59
	12.3' 38"		9.5		
Freezing rate changed at	12.4' 38"		10.064 (Back calculated)		
5.24	12.5' 35"	46"	11.5	1.0	217.39
	12.6' 21"		12.5		
Freezing rate changed at	12.6' 45"		13.021 (Back calculated)		
5.16	12.7' 27"	5'34"	13.1	1	27.47
	12.13'01"		14.1		
Freezing rate changed at	12.14'02"		14.267 (Back calculated)		
5.27	12.14'42"	34"	15.5	1	294.39
	12.15'16"		16.5		

Table :A.7 Run : 3 (ingot : 3 i.e. 4ωt% Bi in Sn)

Potentiometer setting	Real time	Time interval	Cathetometer readings in cms	Diff between cathetometer readings in cms	actual freezing in rate μm/s
	0		8.372		
5.175	2.28' 54"	8'40"	8.5	2.5	48.07
	2.37' 34"		11		
Freezing rate changed at	2.38' 12"		11.183 (Back calculated)		
5.205	2.39' 19"	2'37"	11	2	127.38
	2.41' 56"		14		
Freezing rate changed at	2.42' 21"		14.318 (Back calculated)		
5.17	2.43' 01"	8'10"	15.5	2.5	51.02
	2.51' 11"		17		
Freezing rate changed at	2.51' 47"		17.184 (Back calculated)		
5.25	2.52' 42"	1'16"	18	2.0	263.16
	2.53' 32"		20		

Table :A.8 Run : 4 (ingot : 4 i.e. 1wt% Bi in Sn)

Potentiometer setting	Real time	Time interval	Cathetometer readings in cms	Diff between cathetometer readings in cms	actual freezing rate in μm/s
	0		7.819		
5.205	2.26' 30"	3' 1"	8	2.5	138.12
	2.29' 31"		10.5		
Freezing rate changed at	2.29' 51"		10.776 (Back calculated)		
5.24	2.30' 21"	1.28"	11.5	2.0	227.27
	2.31' 49"		13.5		
Freezing rate changed at	2.32' 11"		13.999 (Back calculated)		
5.16	2.33' 13"	10' 26"	14.2	2.5	39.93
	2.43' 39"		16.7		
Freezing rate changed at	2.44' 01"		16.797 (Back calculated)		
5.27	2.44' 37"	51"	18	1.5	294.11
	2.45' 28"		19.5		

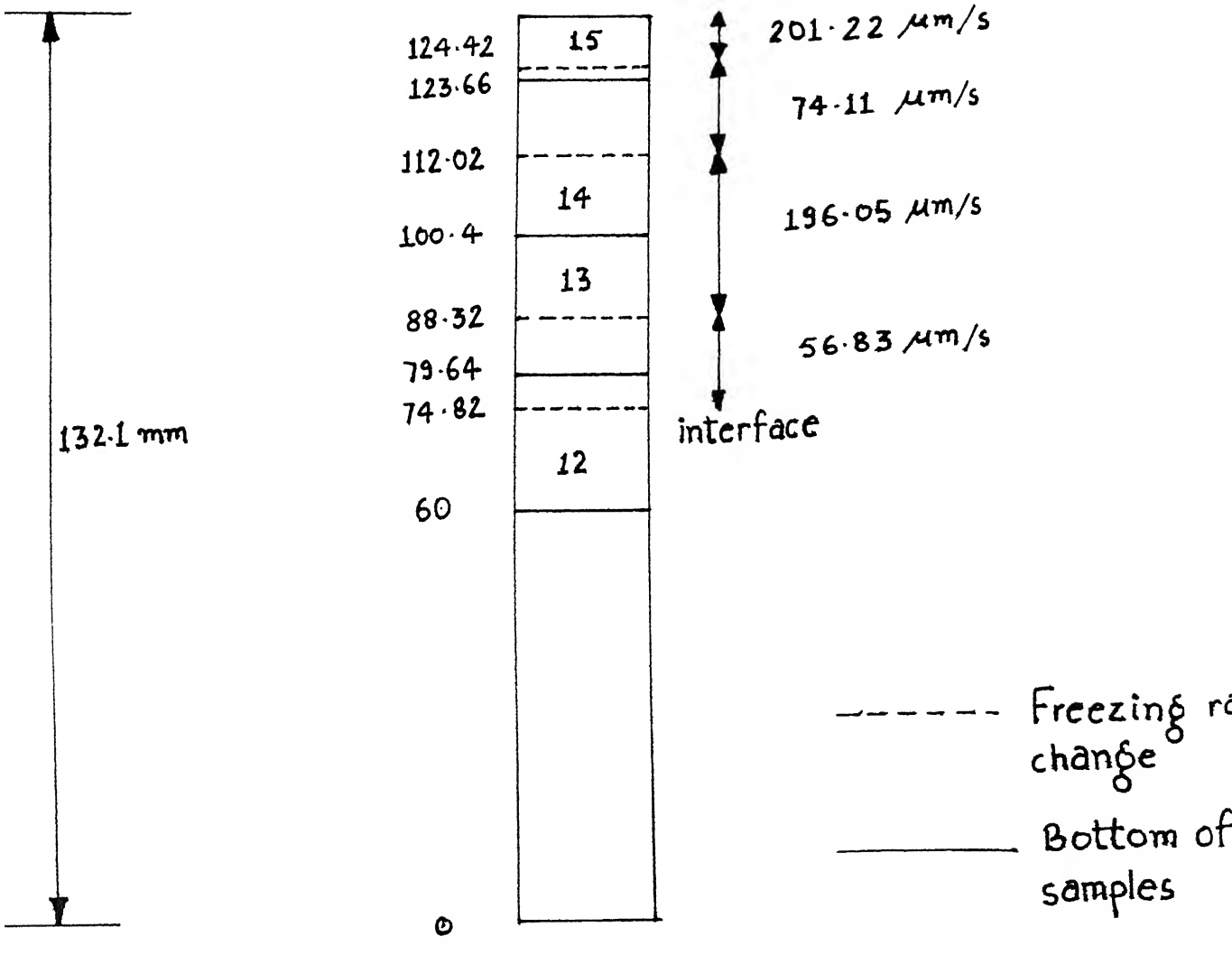

Fig A.1: Schematic diagram of ingot:1

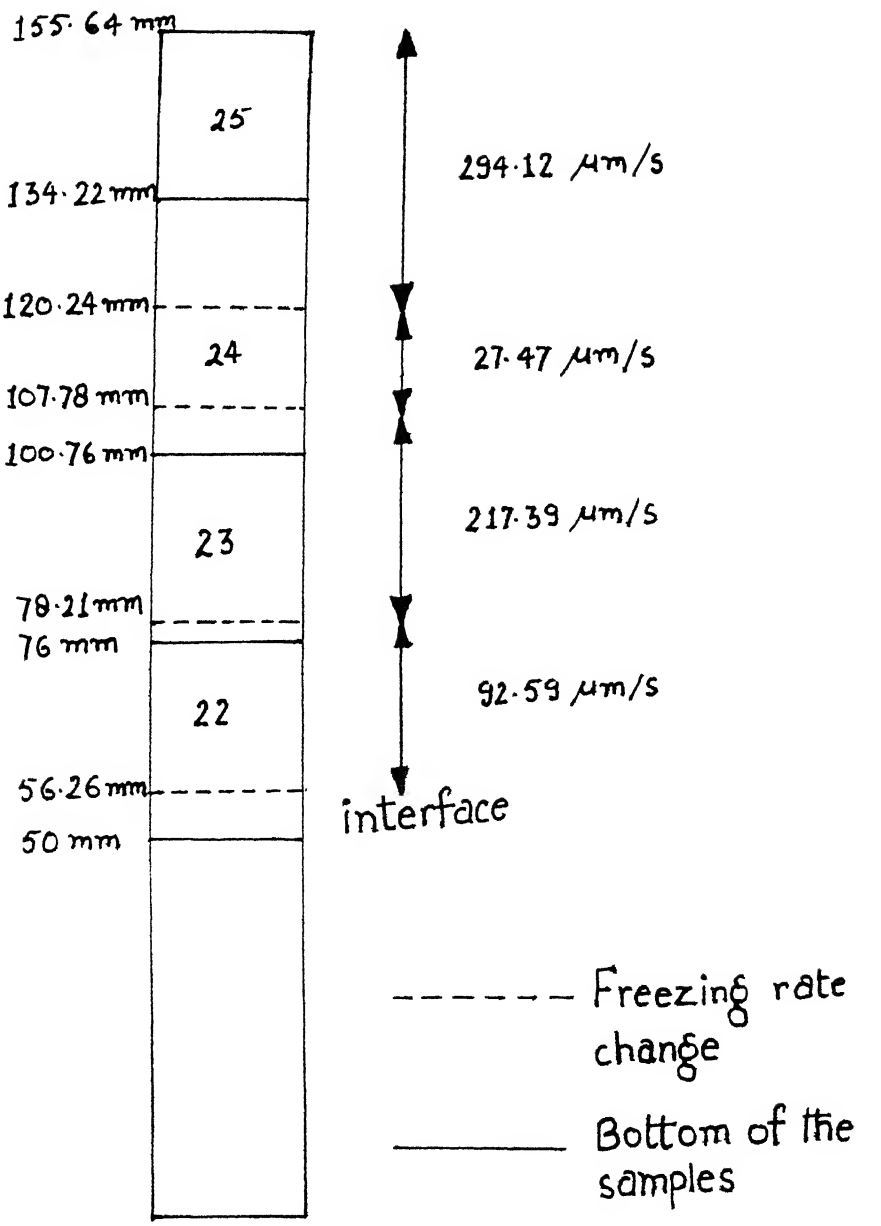

Fig A·2: Schematic diagram of ingot : 2

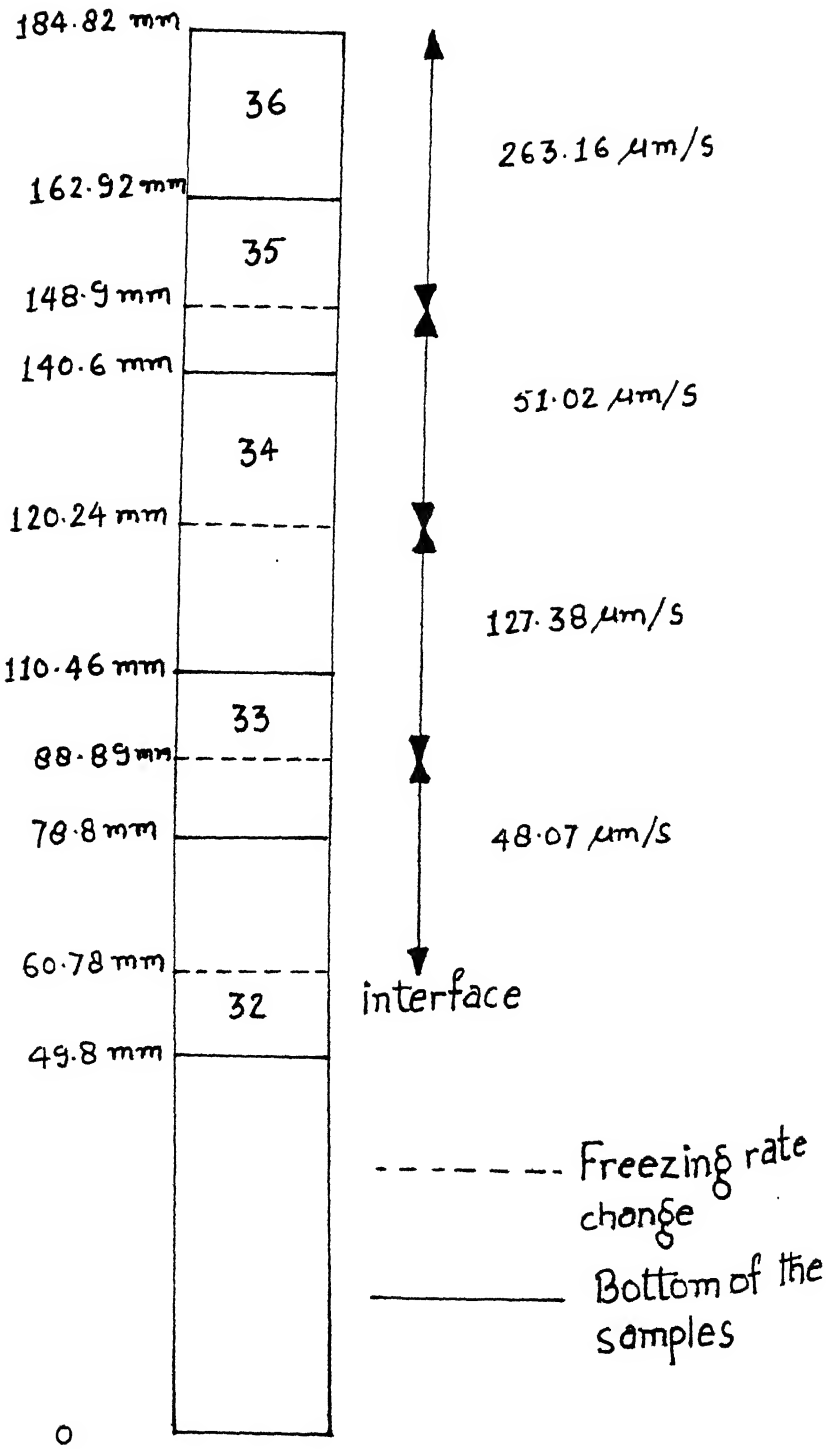

Fig A.3 : Schematic diagram of ingot : 3

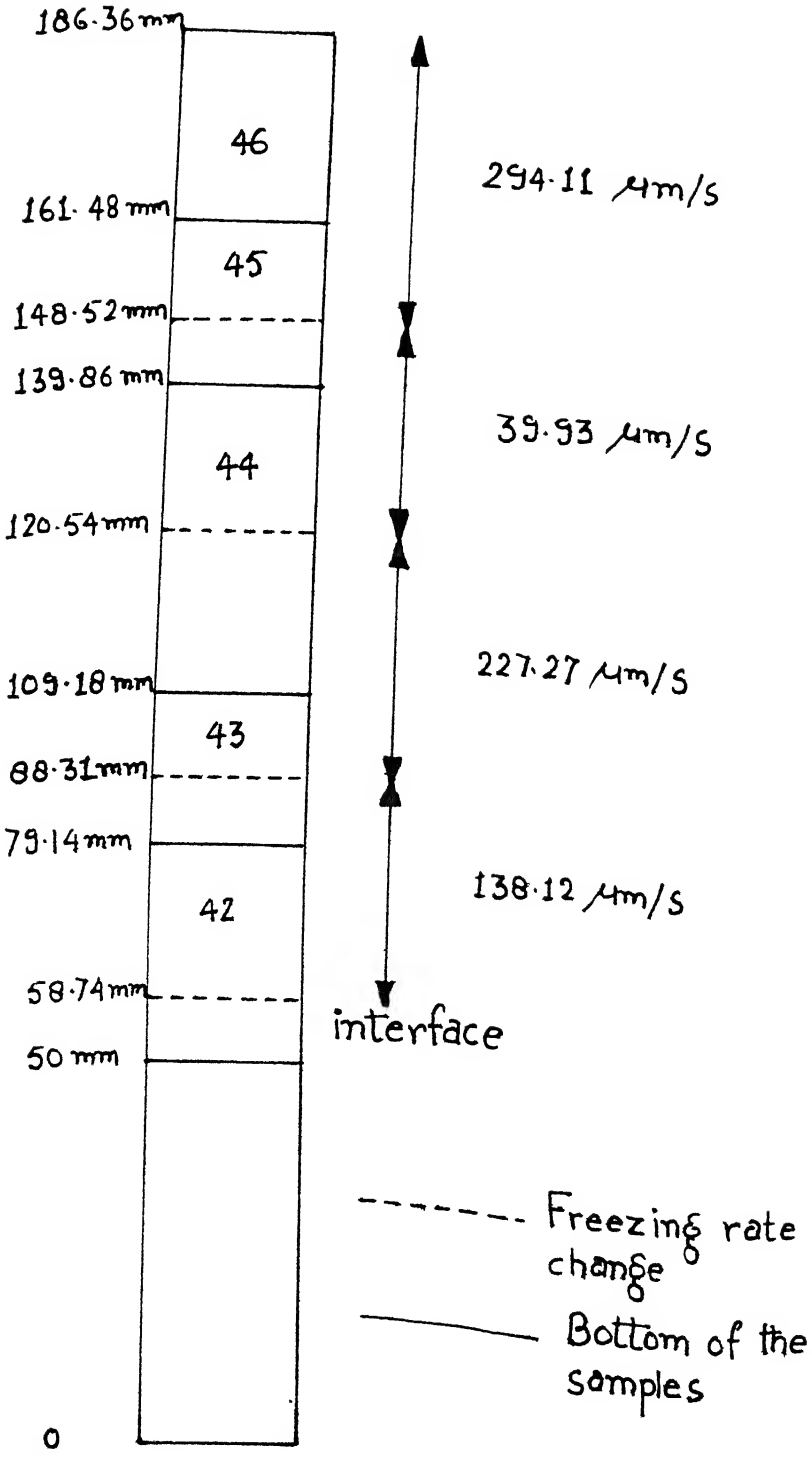

Fig A·4: Schematic diagram of ingot: 4

APPENDIX : 4

Procedure to determine true lamellar dendrite spacing

Fig. A shows two mutually perpendicular sections of a directionally solidified specimen with the direction of heat extraction along the z axis. PM and PL are the traces of a platelike dendrite in the sectioning surfaces A and B. PQ denotes a direction in the surface A and normal to PM, along which the apparent P.D.S, λ, is measured.

If λ_o = is the true spacing then

$$\lambda_o = \lambda K$$

$$\text{where } K = \frac{\sin\theta b}{(1-\cos^2\theta a \cos^2\theta b)^{1/2}}$$

θb = angle which the platelike dendrites make with the longitudinal edge.

θa= angle which the platelike dendrites make with the transverse edge.

This formula proposed by V. Bansal[14] is applicable to the P.D.S measurements on transverse section. The present work involves measurements on longitudinal sections. Considering the geometry of the figure the reverse is true for determining K factor in case of longitudinal sections. Now θb instead of the angle made by the dendrites with the edge of longitudinal section becomes the angle made by the platelike dendrites with the edge of the transverse section. This is true for θa also.

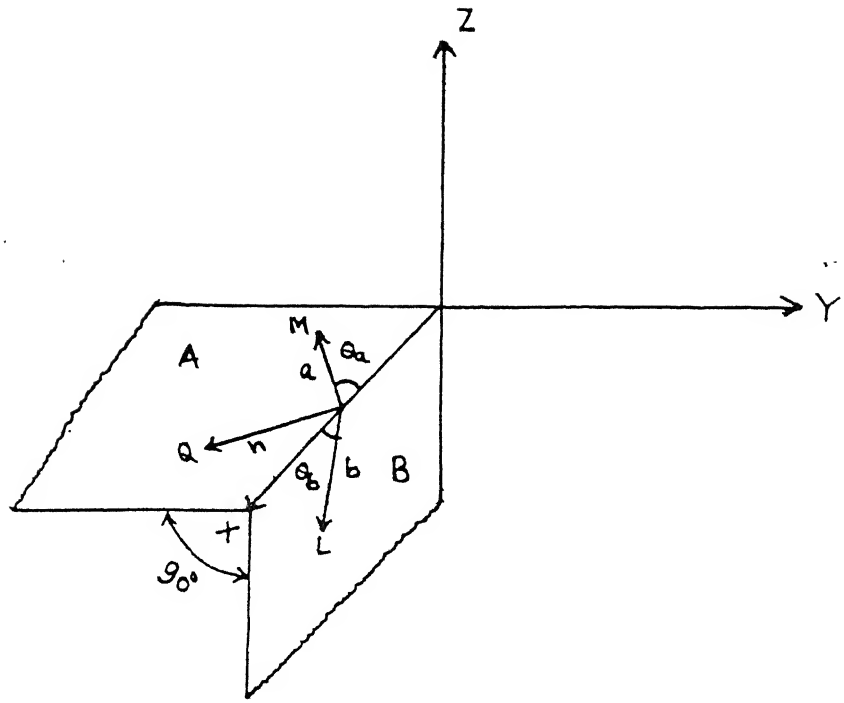

FIG A.5

The transverse(A) and longitudinal (B) sections in a right-handed Cartesian co-ordinate system.

APPENDIX : 5

Measurement of Primary Dendrite Spacing (P.D.S)

Table A9 P.D.S. Measurement Data on ingot : 1

Composition wt% Bi	Sample identification	Freezing rate in μm/s	Distance from starting interface mm	Micrometric reading			Dendrite count (n)	Apparent P.D.S in μm $\frac{x(1.075)}{n}$	K	Real P.D.S in μm
				Initial	Final	Difference (x)				
1	2	3	4	5	6	7	8	9	10	11
	12	56.83	2.1	396	778	382	5	82.13	0.994	81.64
	"	"	2.5	375	754	379	5	81.48	"	80.99
	"	"	3.3	145	881	736	10	79.12	"	78.65
	13	"	4.82	458	821	363	5	78.05	"	77.58
	"	"	5.62	119	834	715	10	76.86	"	76.39
	"	"	6.72	77	732	655	9	78.24	"	77.77
	"	"	8.22	116	768	652	9	77.88	"	77.41
	"	196.05	9.12	250	784	534	9	63.78	"	63.39
	"	"	10.42	162	773	711	12	54.74	"	54.41
	"	"	11.72	104	896	792	16	53.21	"	52.89
	"	"	12.62	36	840	804	16	54.02	"	53.69
	13	196.05	13.92	28	897	869	19	49.17	"	48.87
	"	"	15.32	88	872	784	17	49.57	"	49.27
	"	"	16.72	70	789	719	16	48.31	"	48.02
	"	"	18.32	101	802	701	16	47.09	"	46.81
	"	"	19.82	175	825	650	15	46.58	"	46.3
	"	"	21.42	143	802	659	15	47.23	"	46.95
	14	"	26.08	71	869	798	16	53.61	0.816	43.74
	"	"	27.38	17	842	825	16	55.43	"	45.23
	"	"	28.58	20	834	814	16	54.69	"	44.62
	"	"	29.68	40	881	841	17	53.18	"	43.39

Table 49 contd.

1	2	3	4	5	6	7	8	9	10	11
	14	74.11	30.58	34	869	835	16	56.10	0.816	45.78
	"	"	31.68	26	860	834	16	56.03	"	45.72
	"	"	32.58	42	871	829	16	55.69	"	45.44
	"	"	32.88	21	860	839	16	56.37	"	45.99
	"	"	33.68	59	558	499	9	59.60	"	48.63
	"	"	34.48	18	654	636	11	62.15	"	50.71
	"	"	32.58	20	834	836	16	54.69	"	44.62
	"	"	32.88	40	881	841	17	53.18	"	43.39
	"	"	35.58	41	746	705	10	75.78	"	61.84
	"	"	36.68	8	567	559	8	75.08	"	61.27
	"	"	37.38	63	895	832	12	74.53	"	60.82
	"	"	38.68	30	351	321	12	73.52	"	59.99
	"	"	39.48	60	856	796	12	71.27	"	58.16
1	14	"	40.78	35	491	456	7	70.03	"	57.14
	"	"	41.58	69	877	808	12	72.38	"	59.06
	"	"	42.68	23	528	525	8	70.55	"	57.57
	"	"	43.48	1	480	479	7	73.52	"	59.69
	"	"	44.68	59	862	803	12	71.93	"	58.69
	"	"	46.28	82	890	808	12	72.38	"	59.06
	15	201.22	50.24	42	645	603	11	58.92	"	48.08
	"	"	51.14	4	856	852	15	61.06	"	49.82
	"	"	52.04	37	863	826	14	63.43	"	51.75
	"	"	52.94	53	866	813	14	62.43	"	50.94
	"	"	53.74	45	852	807	15	57.84	"	47.19

Table 9 contd.

1	2	3	4	5	6	7	8	9	10	11
	"	"	54.94	59	823	764	14	58.66	"	47.87
	"	"	58.24	31	894	863	16	57.98	"	47.31

Table A-10 P.D.S. Measurement Data on ingot : 2

Composition wt% Bi	Sample identification	Freezing rate in μm/s	Distance from starting interface mm	Micrometric reading			Dendrite count (n)	Apparent P.D.S in μm x(1.075) / n	K	Real P.D.S in μm
				Initial	Final	Difference (x)				
1	2	3	4	5	6	7	8	9	10	11
	22	92.59	5.5	194	665	471	5	101.27	0.997	100.97
	"	"	6.3	121	608	487	5	104.71	"	104.39
	"	"	7.5	20	487	478	5	102.77	"	102.46
	"	"	8.4	37	512	475	5	101.13	"	101.82
	"	"	9.3	102	666	564	6	101.05	"	100.75
	"	"	10.5	161	628	467	5	100.41	"	100.11
	"	"	11.4	187	452	465	5	99.96	"	99.66
	"	"	13.9	103	558	452	5	97.18	"	96.89
	"	"	17.7	119	715	596	7	91.53	"	91.26
4	23	"	20.24	64	992	928	12	85.13	"	84.87
	"	"	21.44	65	941	876	11	85.61	"	85.35
	"	"	22.54	157	886	729	9	87.08	"	86.82
	"	217.39	23.26	112	797	685	9	81.92	"	81.67
	"	"	24.94	80	762	682	9	81.46	"	81.22
	"	"	26.14	179	859	680	9	81.22	"	80.98
	"	"	27.54	20	620	600	8	80.62	"	80.38
	"	"	28.94	8	821	813	11	79.45	"	79.21
	"	"	30.54	50	712	662	9	79.07	"	78.88
	"	"	31.94	188	865	677	9	80.86	"	80.62
	"	"	33.54	178	902	724	10	77.83	"	77.59
	"	"	35.14	146	872	726	10	78.05	"	77.82

Table 10 contd.

1	2	3	4	5	6	7	8	9	10	11
	"	"	36.44	100	823	723	10	77.72	"	77.49
	"	"	37.54	50	479	429	6	76.86	"	76.63
	"	"	38.94	252	673	421	6	75.43	"	75.20
	"	"	43.04	93	729	636	9	75.96	"	75.73
	24	"	45.7	20	899	879	11	85.90	0.879	75.51
	"	"	47	1	896	895	11	87.47	"	76.89
	"	"	48.2	0	801	801	10	86.11	"	75.69
	"	"	48.8	65	900	835	10	89.76	"	78.39
	"	27.47	49.9	67	923	856	8	115.03	"	101.11
	"	"	51.2	94	955	861	8	115.69	"	101.89
	"	"	51.9	44	830	786	7	120.71	"	106.13
	"	"	54.3	78	985	907	8	121.88	"	107.13
	"	"	55.9	3	705	702	6	125.76	"	110.54
	"	"	57.2	30	766	736	6	131.86	"	115.9
	"	"	58.4	144	798	654	5	140.61	"	123.59
	"	"	59.9	116	778	662	5	142.33	"	125.11
	"	"	61.2	78	734	656	5	141.04	"	123.97
	"	"	62.4	18	596	578	4	155.34	"	136.54
	"	"	63.8	115	701	586	4	157.48	"	138.42
	"	"	65	81	675	594	4	159.64	"	140.32
	"	"	66.2	75	523	448	3	160.53	"	141.11
	"	294.12	67.2	0	402	402	4	108.04	"	94.97
	"	"	68.4	31	471	390	5	83.85	"	73.70
	"	"	69.2	74	452	378	5	81.27	"	71.44

Table 10 contd.

1	2	3	4	5	6	7	8	9	10	11
	"	"	70.4	135	584	449	6	80.46	"	70.72
	"	"	71.2	100	551	451	6	80.80	"	71.02
	"	"	72.2	126	577	451	6	80.80	"	71.02
	"	"	73.5	160	573	413	6	73.99	"	65.04
	"	"	74.2	161	571	510	6	73.46	"	64.57
	"	"	75.9	170	836	766	10	71.59	"	62.93
	25	"	78.36	376	760	384	7	58.97	0.997	58.79
	"	"	79.96	190	460	270	5	58.05	"	57.87
	"	"	84.86	214	525	311	6	55.72	"	55.56
	"	"	88.06	335	649	314	6	56.26	"	56.09
	"	"	91.16	390	648	258	5	55.47	"	55.30
	"	"	95.46	474	729	255	5	54.83	"	54.67
	"	"	96.26	485	741	256	5	55.04		54.87

Table 11 P.D.S. Measurement Data on ingot : 3

Composition wt% Bi	Sample identification	Freezing rate in μm/s	Distance from starting interface mm	Micrometric reading			Dendrite count (n)	Apparent P.D.S in μm x(1.075) / n	K	Real P.D.S in μm
				Initial	Final	Difference (x)				
	32	48.07	1.7	67	658	591	6	105.88	0.999	105.77
	"	"	5.6	41	625	584	6	104.63	"	104.53
	"	"	6.9	15	685	670	7	102.89	"	102.79
	"	"	8.3	203	866	663	7	101.82	"	101.72
	"	"	9.4	1	948	947	10	101.80	"	101.69
	"	"	11.1	32	965	933	10	100.3	"	100.19
	33	127.38	32.12	152	673	521	5	112.02	0.648	72.59
	"	"	32.82	231	750	519	5	111.59	"	[illegible]
	"	"	34.02	211	816	605	6	108.36	"	70.22
2	"	"	35.12	45	820	775	8	104.14	"	67.48
	"	"	36.52	163	545	382	4	102.66	"	66.52
	"	"	37.72	319	890	571	6	102.30	"	66.29
	"	"	38.92	287	945	658	7	101.05	"	65.48
	"	"	40.32	338	805	467	5	100.41	"	65.07
	"	"	41.62	34	779	745	8	100.11	"	64.87
	"	"	43.72	101	845	744	8	99.98	"	64.79
	34	"	51.38	23	725	702	8	94.33	0.677	63.86
	"	"	52.18	92	793	701	8	94.19	"	63.76
	"	"	53.48	326	781	455	5	97.83	"	66.23
	"	"	54.28	220	768	548	6	98.18	"	66.46
	"	"	55.38	20	564	544	6	97.47	"	65.99
	"	"	56.78	157	702	545	6	97.65	"	66.11

Table 11 contd.

2	3	4	5	6	7	8	9	10	11
"	"	58.18	25	565	540	6	96.75	"	65.49
"	"	59.48	33	481	448	5	96.32	"	65.21
"	"	60.78	260	697	437	5	93.96	"	63.61
"	51.02	62.18	53	860	807	7	123.93	"	83.90
"	"	63.38	54	883	829	7	127.31	"	86.19
"	"	64.88	221	922	701	6	125.59	"	85.02
"	"	66.28	162	868	706	6	126.49	"	85.63
"	"	67.38	190	785	595	5	127.92	"	86.60
"	"	69.98	119	736	617	5	132.66	"	89.81
"	"	73.08	118	756	638	5	137.17	"	92.86
"	"	74.38	62	713	651	5	139.97	"	94.76
"	"	76.45	72	735	663	5	142.56	"	96.51
35	"	79.82	210	802	592	6	106.06	0.893	94.71
"	"	80.42	274	867	593	6	106.25	"	94.88
"	"	80.92	250	840	590	6	105.71	"	94.39
"	"	82.32	320	815	495	5	106.43	"	95.04
"	"	83.22	194	687	493	5	105.99	"	94.65
"	"	84.62	122	620	498	5	107.07	"	95.70
"	"	85.72	197	801	604	6	108.22	"	96.64
"	"	87.02	281	888	607	6	108.75	"	97.11
"	263.16	88.62	189	765	576	7	88.46	"	78.99
"	"	90.02	14	717	703	9	83.97	"	74.99
"	"	91.52	37	699	662	9	79.07	"	70.61
"	"	92.62	72	730	658	9	78.59	"	70.18
"	"	93.32	391	740	359	5	77.17	"	68.93

Table A1 contd.

2	3	4	5	6	7	8	9	10	11
"	"	94.12	198	841	643	9	76.80	"	68.58
"	"	95.22	110	836	726	10	78.05	"	69.69
"	"	96.12	325	805	480	7	73.71	"	65.82
"	"	97.62	128	525	397	6	71.13	"	63.52
"	"	99.02	134	590	456	7	70.03	"	62.54
36	"	102.04	94	646	552	11	53.95	0.998	53.84
"	"	102.94	292	861	569	11	55.61	"	55.49
"	"	104.74	255	862	607	12	54.38	"	54.27
"	"	106.84	167	878	711	15	53.96	"	53.85
"	"	109.24	264	871	607	13	53.19	"	53.08
"	"	114.14	55	870	815	16	54.76	"	54.65
"	"	119.24	64	865	801	16	53.82	"	53.71
"	"	121.44	204	858	654	13	54.08	"	53.97

Table 12 P.D.S. Measurement Data on ingot : 4

Impo-tion % Bi	Sample identi-fication	Freezing rate in μm/s	Distance from starting interface mm	Micrometric reading			Dendrite count (n)	Apparent P.D.S in μm x(1.075) / n	K	Real P.D.S in μm
				Initial	Final	Difference (x)				
	2	3	4	5	6	7	8	9	10	11
1	42	138.12	0.8	473	665	192	3	68.8	0.912	62.74
	"	"	2.3	138	518	380	6	68.08	"	62.09
	"	"	3.2	62	510	448	7	68.8	"	62.74
	"	"	4.7	9	761	752	12	67.37	"	61.44
	"	"	5.9	20	739	719	12	64.41	"	58.74
	"	"	7.3	65	773	708	12	63.43	"	57.85
	"	"	9	83	850	767	13	63.43	"	57.85
	"	"	10.8	65	846	781	14	59.97	"	54.69
	"	"	12.1	42	772	730	13	60.37	"	55.06
	"	"	13.2	20	844	824	15	59.05	"	53.85
	"	"	14.4	23	805	782	14	60.05	"	54.77
	"	"	15.7	76	849	773	14	59.36	"	54.14
	"	"	17.3	109	665	556	10	59.77	"	54.51
	43	"	22.2	0	908	908	16	61.01	0.849	51.79
	"	"	23.4	13	918	905	16	60.80	"	51.45
	"	"	24.3	38	944	906	16	60.87	"	51.68
	"	"	25	31	855	824	15	59.05	"	50.13
	"	"	26.2	11	840	829	15	59.21	"	50.44
	"	"	27.3	21	918	897	16	60.27	"	51.17
	"	"	28.1	24	926	902	16	60.60	"	51.45
	"	227.27	29.4	18	867	849	17	53.67	"	45.58
	"	"	30.3	47	868	821	17	51.92	"	44.08

Table A12 contd.

2	3	4	5	6	7	8	9	10	11
"	"	31.4	0	849	849	17	53.69	"	45.58
"	"	32.9	1	784	783	16	52.61	"	44.67
"	"	34.2	28	829	801	17	50.65	"	43.00
"	"	35.4	33	827	794	17	50.21	"	42.63
"	"	36.8	41	867	826	18	49.33	"	41.88
"	"	38.3	28	853	825	18	49.27	"	41.83
"	"	39.2	54	845	791	17	50.02	"	42.47
"	"	40.5	85	869	784	17	49.58	"	42.09
"	"	41.9	3	918	915	20	49.18	"	41.75
"	"	43.3	20	855	835	18	49.87	"	42.34
"	"	45.2	58	850	792	17	50.08	"	42.52
"	"	48	19	866	847	18	50.58	"	42.94
44	"	50.84	60	867	807	18	48.16	0.883	42.53
"	"	51.74	90	855	765	17	48.38.	"	42.72
"	"	52.94	92	861	769	17	48.63	"	42.94
"	"	53.84	62	828	766	17	48.44	"	42.77
"	"	54.64	49	866	817	18	48.79	"	43.08
"	"	55.74	70	738	668	15	47.87	"	42.27
"	"	56.84	132	838	706	16	47.43	"	41.88
"	"	57.74	135	805	670	15	48.02	"	42.4
"	39.93	59.64	1	820	819	13	67.73	"	59.81
"	"	60.84	6	856	850	13	70.29	"	62.07
"	"	62.24	41	840	799	11	78.08	"	68.94
"	"	63.74	76	831	755	10	81.16	"	71.66
"	"	65.54	48	861	813	11	79.45	"	70.15

Table 12 contd.

1	2	3	4	5	6	7	8	9	10	11
	"	"	66.84	56	870	814	11	79.55	"	70.24
	"	"	68.34	49	802	753	10	80.95	"	71.48
	"	"	69.74	22	783	761	10	81.81	"	72.24
	"	"	71.94	37	871	834	11	81.5	"	71.96
	"	"	72.64	41	893	852	11	83.26	"	73.52
	"	"	74.94	28	822	794	10	85.36	"	75.37
	"	"	76.64	34	841	807	10	86.75	"	76.6
	"	"	78.94	56	878	822	10	88.36	"	78.03
	45	"	82.02	63	578	515	6	92.27	0.904	83.41
	"	"	83.42	53	837	784	9	93.64	"	84.65
	"	"	84.22	44	656	612	7	93.99	"	84.97
	"	"	85.42	57	847	790	9	94.36	"	85.30
	"	"	86.32	34	738	704	8	94.6	"	85.52
	"	"	87.22	175	793	618	7	94.91	"	85.79
	"	"	88.52	173	795	622	7	95.52	"	86.35
	"	"	89.32	34	745	711	8	95.54	"	86.37
	"	294.11	90.42	152	820	668	11	65.28	"	59.01
	"	"	91.32	163	762	599	11	58.54	"	52.92
	"	"	92.22	98	734	636	12	56.98	"	51.51
	"	"	93.92	103	729	626	12	56.08	"	50.69
	"	"	95.52	112	783	671	13	55.48	"	50.15
	"	"	96.82	85	727	642	13	53.09	"	47.99
	"	"	99.22	27	862	835	17	52.80	"	47.73
	"	"	101.12	65	880	815	17	51.54	"	46.59
	46	"	105.9	13	716	703	10	41.98	0.999	41.94

Table A12 contd.

2	3	4	5	6	7	8	9	10	11
"	"	107.5	58	792	734	19	41.53	"	41.49
"	"	110	83	811	728	19	41.9	"	41.15
"	"	112.6	117	802	685	18	40.91	"	40.93
"	"	115.4	46	772	726	19	41.08	"	41.04
"	"	117.8	39	794	755	20	40.58	"	40.54
"	"	120.2	56	803	747	20	40.15	"	40.11
"	"	121.7	72	851	779	21	39.88	"	39.84
"	"	124.8	32	841	809	22	39.53	"	39.49

APPENDIX : 6

Angle measurement data

Table A-13

Ingot No	Sample identification No	Angle made by dendrites with longitudinal edge θ_a in degrees	Angle made by dendrites with transverse edge θ_b in degrees	$K = \frac{\sin\theta_b}{(1-\cos^2\theta_a \cos^2\theta_b)^1}$
1	12	87	83.5	0.994
1	13	87	83.5	0.994
1	14	77	54	0.816
1	15	77	54	0.816
2	22	85.5	85	0.997
2	23	87.5	85.5	0.997
2	24	87.5	61.5	0.879
2	25	89	86	0.997
3	32	88.5	87	0.999
3	33	80.5	40	0.648
3	34	74	41.5	0.677
3	35	68.5	61.5	0.893
3	36	68.5	87	0.998
4	42	75	65	0.912
4	43	70	57	0.849
4	44	78.5	61.5	0.883
4	45	67.5	63	0.904
4	46	64.5	87	0.999